

Response to reviewers

We have thoroughly responded to the four reviewer's comments in four specific files. We believe we have addressed all comments of the reviewers and we thus have uploaded a final version of the paper accounting for the suggested changes they have made.

Best Regards,

Philippe Peylin

1 **A new step-wise Carbon Cycle Data Assimilation System**
2 **using multiple data streams to constrain the simulated land**
3 **surface carbon cycle**

4

5 | **P. Peylin¹, C. Bacour², N. MacBean¹, S. Leonard¹, P. J. Rayner^{1,3}, S. Kuppel^{1,4}, E.**
6 | **N. Koffi¹, A. Kane¹, F. Maignan¹, F. Chevallier¹, P. Ciais¹, P. Prunet²**

7 [1]{Laboratoire des Sciences du Climat et de l'Environnement, UMR 8212 CEA-CNRS-
8 UVSQ, 91191 Gif-sur-Yvette cedex, France}

9 [2]{Noveltis, Parc Technologique du Canal, 2 avenue de l'Europe, 31520 Ramonville-Saint-
10 Agne, France}

11 [3]{University of Melbourne, 3010, Vic, Melbourne, Australia}

12 [4]{[Grupo de Estudios Ambientales, IMASL-CONICET/Universidad Nacional de San Luis,](#)
13 [San Luis, Argentina](#)}

14 Correspondence to: P. Peylin (philippe.peylin@lsce.ipsl.fr)

15

16

Philippe Peylin 8/3/16 18:16
Mis en forme: Police :(Par défaut) Times
New Roman, 12 pt, Couleur de police :
Noir, Anglais (E.U.)

1 Abstract

2 Large uncertainties in Land surface models (LSMs) simulations still arise from inaccurate
3 forcing, poor description of land surface heterogeneity (soil and vegetation properties),
4 incorrect model parameter values and incomplete representation of biogeochemical processes.
5 The recent increase in the number and type of carbon cycle related observations, including
6 both in situ and remote sensing measurements, has opened a new road to optimize model
7 parameters via robust statistical model-data integration techniques, in order to reduce the
8 uncertainties of simulated carbon fluxes and stocks. In this study we present a Carbon Cycle
9 Data Assimilation System (CCDAS) that assimilates three major data streams, namely
10 MODIS-NDVI observations of vegetation activity, net ecosystem exchange (NEE) and latent
11 heat (LE) flux measurements at more than 70 sites (FLUXNET), and atmospheric CO₂
12 concentrations at 53 surface stations, in order to optimize the main parameters of the
13 ORCHIDEE LSM (around 180 parameters in total). The system relies on a step-wise
14 approach that assimilates each data stream in turn, propagating the information gained on the
15 parameters from one step to the next.

16 Overall, the ORCHIDEE model is able to achieve a consistent fit to all three data streams,
17 which suggests that current LSMs have reached the level of development to assimilate these
18 observations. The assimilation of MODIS-NDVI (step 1) reduced the growing season length
19 in ORCHIDEE for temperate and boreal ecosystems, thus decreasing the global mean annual
20 gross primary production (GPP). Using FLUXNET data (step 2) led to large improvements in
21 the seasonal cycle of the NEE and LE fluxes for all ecosystems (i.e., increased amplitude for
22 temperate ecosystems). The assimilation of atmospheric CO₂, using the atmospheric transport
23 model LMDz (step 3), provides an overall constraint (i.e., constraint on large scale net CO₂
24 fluxes), resulting in an improvement of the fit to the observed atmospheric CO₂ growth rate.
25 Thus the optimized model predicts a land C sink of around 2.2 PgC.yr⁻¹ (for the 2000-2009
26 period), which is more compatible with current estimates from the Global Carbon Project
27 (GCP) than the prior value. The consistency of the step-wise approach is evaluated with back-
28 compatibility checks. The final optimized model (after step 3) does not significantly degrade
29 the fit to MODIS-NDVI and FLUXNET data that were assimilated in the first two steps,
30 suggesting that a stepwise approach can be used instead of the more “challenging”
31 implementation of a simultaneous optimization in which all data streams are assimilated
32 together. Most parameters, including the scalar of the initial soil carbon pool size, changed

Philippe Peylin 3/6/16 09:35

Supprimé: uncertainties

1 during the optimization with a large error reduction. This work opens new perspectives for
2 better predictions of the land carbon budgets.

3

4 **1 Introduction**

5 Atmospheric CO₂ concentrations have increased at an unprecedented rate over the last few
6 decades, predominantly due to anthropogenic fossil fuel and cement emissions, as well as
7 land use and land cover change (LULCC). The oceans and the terrestrial biosphere have
8 absorbed CO₂, removing on average 50% of anthropogenic emissions from the atmosphere.
9 However, knowledge about the exact location of sources and sinks of carbon (C) and the
10 driving mechanisms is still lacking. Land surface models (LSMs) can be used to improve our
11 understanding of the spatio-temporal patterns of sources and sinks, as well as for attributing
12 changes due to CO₂, climate variability and other environmental drivers. However, the spread
13 in the model predictions of terrestrial net C exchange currently has the same order of
14 magnitude as the uncertainty of the terrestrial C budget estimated as the residual of the other
15 carbon cycle components (Le Quéré et al., 2015). In addition to uncertainties in the mean
16 global annual terrestrial C budget and its trend over time (Sitch et al., 2015), there remain
17 strong discrepancies between LSMs in their predictions of regional budgets (Canadell, 2013)
18 at seasonal and inter-annual timescales and in their sensitivity to climate and atmospheric CO₂
19 forcing (Piao et al., 2013).

20 Uncertainties in model simulations arise from inaccurate forcing, incorrect model parameter
21 values and/or an inadequate or incomplete representation of biogeochemical processes in the
22 model (for example the impact of nutrient limitation on C fluxes, or C release related to
23 permafrost thawing). Arguably the best way to improve model predictions is to confront
24 simulations with multiple sources of data within an appropriate and rigorous framework
25 (Prentice et al., 2015). In the last two decades significant efforts by the site and satellite
26 observation communities have resulted in a large increase in the number and type of C cycle-
27 related observations. These data contain some information at various spatial and temporal
28 scales and should be combined together to robustly address different aspects of the models.
29 One way in which these data can be used to better quantify and reduce model uncertainty is
30 by optimizing or calibrating the model parameters via robust statistical model-data fusion (or
31 data assimilation – DA) techniques. In particular a Bayesian inference framework allows us to

Philippe Peylin 10/6/16 19:41

Supprimé: s

1 update our prior knowledge of the parameters based on new information contained in the
2 observations.

3 There is a long history of using DA techniques for parameter optimization, particularly in
4 Geophysics (Tarantola, 1987), but the initial studies in the field of global terrestrial C cycle
5 data assimilation started with the initial study of Fung et al. (1987) and a pioneering work by
6 Knorr and Heimann (1995) who used atmospheric CO₂ concentration to constrain the Simple
7 Diagnostic Biosphere Model (SDBM). This effort was continued by the original Carbon
8 Cycle Data Assimilation System (CCDAS) described in Rayner et al. (2005) and Kaminski et
9 al. (2012) which used both atmospheric CO₂ and satellite-derived Fraction of Absorbed
10 Photosynthetic Radiation (FAPAR) data to optimize vegetation productivity by adjusting the
11 C cycle-related parameters of the Biosphere Energy-Transfer Hydrology (BETHY) model
12 (see a review in Kaminski et al., 2013). Meanwhile substantial efforts have been put into the
13 use of local eddy covariance flux tower measurements of net exchange of CO₂ and latent and
14 sensible heat fluxes to optimize photosynthesis, respiration and energy-related parameters of
15 terrestrial ecosystem models, both at individual sites (e.g. Wang et al., 2001, 2007; Williams
16 et al., 2005; Braswell et al., 2005; Knorr and Kattge, 2005; Moore et al., 2008; Ricciuto et al.,
17 2008), and more recently using multiple sites together (hereafter multiple sites) from the
18 global FLUXNET network (e.g. Groenendijk et al., 2011; Kuppel et al., 2012, 2014; Alton,
19 2013; Xiao et al., 2014). Increasingly the focus in carbon cycle data assimilation is moving
20 towards using multiple different data streams as independent constraints, with the aim of
21 bringing more information at different spatial and temporal scales and constraining several
22 processes at once in order to reduce the likelihood of model equifinality (where multiple sets
23 of parameters achieve the same reduction in model-data misfit). Recent examples include the
24 combination of in-situ eddy covariance flux observations and ground-based information on
25 vegetation structure and C stocks (Richardson et al., 2010; Ricciuto et al., 2011; Keenan et al.,
26 2012, 2013; Thum et al., 2015), or in-situ flux data and satellite FAPAR (Kato et al., 2013;
27 [Zobitz et al., 2014; Bacour et al., 2015](#) **or atmospheric CO₂ and biomass data using a simple**
28 **biosphere model (Saito et al., 2014)**). This is a non-trivial task however, especially when
29 optimizing a complex LSM (see MacBean et al, submitted), which has many parameters
30 acting from local to global scales.

31 When assimilating multiple different data streams we have two options: i) to optimize the
32 model with each data stream in turn, and to propagate the information gained on the

1 parameter values from one step to the next (hereafter referred to as “stepwise” assimilation),
2 or ii) to include all data streams together in the same optimization (hereafter referred to as
3 “simultaneous” assimilation). Kaminski et al. (2012) suggested that it is essential to perform a
4 consistent, simultaneous assimilation that includes all data streams in the same optimization.
5 It is important to note that this is an implementation question. Tarantola (2005) recasts the
6 fundamentals of the approach as the conjunction or multiplication of probability densities.
7 This multiplication is associative so it makes no difference whether it is performed in one step
8 or several (and whether the system is linear or not). In complex problems such as these, one
9 cannot carry or even describe the full structure of the relevant probability densities so which
10 approach will work best in each case is unclear. In particular, technical difficulties associated
11 with the different number of observations for each data stream and the characterization of
12 error correlations between them, in addition to computational constraints to run global LSMs,
13 might result in the preference for a step-wise assimilation framework. Additionally, it may be
14 more straightforward, to expose a restricted set of parameters (following a global sensitivity
15 analysis) to each observation type in a stepwise approach to ensure that each data stream
16 constrains only the most relevant parts of the model. This reduces biases from other poorly-
17 represented processes caused by inadequate model structure. For these reasons we follow the
18 stepwise approach in this paper.

19 We present the first global-scale CCDAS that assimilates three of the main global data
20 streams that have been used to date to understand the terrestrial carbon cycle – atmospheric
21 CO₂ concentration, satellite-derived information of vegetation greenness (from the MODIS
22 instrument) and multisite eddy covariance net CO₂ and latent heat flux measurements (from
23 FLUXNET) – to optimize the parameters of the Organizing Carbon and Hydrology in
24 Dynamics Ecosystems (ORCHIDEE) process-based LSM (Krinner et al., 2005). The main
25 questions that we aim to answer in this paper are as follows:

- 26 i) How and to which extend the optimization of the ORCHIDEE model allows to fit the three
27 data streams that are considered?
- 28 ii) Does the step-wise optimization result in a degradation of the fit to other data streams used
29 in the previous steps?
- 30 iii) What are the main changes in the optimized parameters when using sequentially these
31 three data streams in a global CCDAS and which processes are constrained?

1 iv) What are the improvements for the land C cycle in terms of net/gross fluxes and stocks as
2 a result of multi-data stream optimization? What preliminary perspectives can we draw that
3 may help us in improving model predictions of trends, variability and the location of
4 terrestrial C sources and sinks?

5 Following these objectives, the paper first describes the new ORCHIDEE-CCDAS including
6 the concept, the observations, the models and the optimization approach. We then present the
7 results, including the fit to the data, consistency checks (question i) above) as well as mean
8 global and regional C cycle budget for the period 2000-2009. The last section discusses issues
9 and perspectives associated with these results.

10

11 **2 Methods**

12 **2.1 ORCHIDEE-CCDAS concept**

13 We have designed a CCDAS around the ORCHIDEE land surface model (ORCHIDEE-
14 CCDAS, later also referred to as ORCHIDAS for simplicity) that combines a state-of-the-art
15 description of the driving biogeochemical processes within the model with multiple
16 observational constraints in a robust statistical framework, in order to improve the simulation
17 of land carbon fluxes and stocks. The system allows us to retrieve the best estimate, given the
18 observations and prior information, of selected parameters (see §2.3.3) as well as to evaluate
19 their uncertainty. It relies on a stepwise assimilation of a comprehensive set of three C cycle-
20 related observations that are representative of small (100 m) to large (continental) scales (see
21 §2.2):

- 22 • Step 1: Satellite measurements of vegetation activity using the Normalized Difference
23 Vegetation Index (NDVI) from the MODIS instrument over the 2000-2008 period for
24 a randomly selected set of sites for boreal and temperate deciduous vegetation types;
- 25 • Step 2: In-situ eddy-covariance net CO₂ and water (latent heat) flux measurements
26 from the FLUXNET database for a large set of sites, spanning 7 different vegetation
27 types;
- 28 • Step 3: In-situ monthly atmospheric surface CO₂ concentration measurements from
29 the GLOBALVIEW-CO₂ database over three years (2002-2004).

30 The system relies on two models:

- 1 • The ORCHIDEE global LSM, whose main C cycle parameters are optimized (see
2 §2.3)
- 3 • The atmospheric transport model, LMDz (see §2.3), to relate the surface carbon fluxes
4 to atmospheric CO₂ concentrations.

5 The framework combines the different observational data streams within ORCHIDAS in
6 order to optimize selected model parameters using a variational data assimilation system,
7 described in section 2.4. Figure 1 illustrates the structure of the CCDAS and the different
8 components that are involved. Such a framework distinguishes i) the assimilated observations,
9 ii) an ensemble of forcing and input data streams, iii) the models and optimization framework,
10 as well as iv) an evaluation step, where independent datasets are compared to the optimized
11 model stocks and fluxes. As explained in the introduction, a major feature of the current
12 system is the stepwise approach, in which all data streams are assimilated sequentially (i.e.
13 one after the other). The information retrieved at a given step (retrieved optimal parameter
14 values and associated uncertainty) is propagated to the next step (see Fig. 2 and §2.4). Note
15 that for simplicity we did not propagate the error correlations in this first implementation of
16 the system ([section 4 discusses the potential impact of this simplification](#)).

17 At each step, the parameter optimization relies on a Bayesian framework that explicitly
18 minimizes the difference between the simulated and observed quantities in addition to
19 minimizing the difference between the optimized model parameters and “a priori” values (see
20 §2.4.2). The dependence of the simulated quantities on the optimized variables is non-linear,
21 which thus necessitates the use of an iterative algorithm. Note that all components of the
22 surface C budget need also to be included in the ORCHIDAS, particularly when using
23 atmospheric CO₂ measurements which requires the atmospheric transport model to be
24 prescribed with fossil fuel emissions, CO₂ fluxes associated with biomass burning and ocean
25 CO₂ fluxes (see §2.5) in addition to net ecosystem exchange (NEE) from ORCHIDEE.

26 **2.2 Assimilated observations**

27 **2.2.1 MODIS-NDVI**

28 MODIS collection 5 obtained from surface reflectance data (from 2000-2008) in the red (R)
29 and near-infrared (NIR) bands at 5 km resolution (CMG) are used to optimize the phenology-
30 related parameters of ORCHIDEE in the first step. The R and NIR data were processed to

Philippe Peylin 3/6/16 11:34

Supprimé: d

1 correct for directional effects following Vermote et al. (2009) and then used to calculate the
2 NDVI, which is assumed to be linearly related to the model FAPAR. The NDVI are then i)
3 aggregated to the 0.72° spatial resolution of the ERA-Interim meteorological fields that are
4 used to force ORCHIDEE, ii) interpolated to a daily time series and iii) checked for quality
5 (see MacBean et al., 2015 for details). If there is a gap in the observations of more than 15
6 days, no interpolation is done (i.e., no data during the gap are assimilated). Figure 3 displays
7 the location of the sites that were selected (see §2.4.1).

8 2.2.2 Eddy covariance flux data

9 Eddy covariance flux measurements of net surface CO₂ flux – hereafter referred to as net
10 ecosystem exchange (NEE) and latent heat flux (LE) – from 78 observation sites of a network
11 of regional networks (FLUXNET; see Fig. 3) are used to constrain ecosystem physiology and
12 fast C-related processes at daily to seasonal timescales in ORCHIDEE in the second step. We
13 use quality-checked and gap-filled data from a global synthesis called the La Thuile dataset
14 (Papale, 2006). In order to avoid dealing with the large error correlations in the half-hourly
15 data (see Lasslop et al., 2008), daily mean values of NEE and LE are used in the ORCHIDAS.
16 Days with less than 80% of the half-hourly data are left out of the assimilation. The selection
17 of the sites and the data processing (gap-filling, correction for energy balance closure) are
18 detailed in Kuppel et al. (2014).

19 2.2.3 Atmospheric CO₂ concentrations

20 Atmospheric CO₂ concentration measurements were taken from an ensemble of selected
21 surface stations around the world (Fig. 3). The spatial concentration gradients relate to the
22 integral of the fluxes over large areas and thus allow the optimization of large-scale global
23 patterns of carbon fluxes. These data were taken from the NOAA Earth System Laboratory
24 (ESRL) GLOBALVIEW-CO₂ collaborative product (GLOBALVIEW-CO₂, 2013) and
25 averaged to monthly means. We assimilated the monthly values for 53 sites for the 2002-2004
26 period inclusive in the last step of the assimilation system. Such restricted period (3 years
27 only) was chosen for practical reasons (computing resources) while constructing the
28 ORCHIDAS system. The station locations, indicated in Fig. 3, favor the background
29 conditions i.e. the surrounding air masses are only weakly influenced by local continental
30 sources, such as power plants. The choice of monthly mean is related to the use of pre-
31 calculated transport fields with LMDZ (see §2.3.2). We also used additional sites to evaluate

1 | the result of the optimization (locations indicated in Fig. 3): 17 sites more representative of
2 | local continental fluxes and 7 sites from Pacific Ocean cruises that were left aside in order not
3 | to overweight that particular region in the optimization.

4 | 2.3 Models and optimized parameters

5 | 2.3.1 ORCHIDEE land surface model

6 | In this study we use the ORCHIDEE process-oriented land surface model (Krinner et al.,
7 | 2005), which computes water, carbon and energy balances at the land surface on a half hourly
8 | time step, using a mechanistic description of the physical and biogeochemical processes (see,
9 | <http://labex.ipsl.fr/orchidee/>). The model describes the exchange of carbon and water at the
10 | leaf level, the allocation of carbon within plant compartments (leaves, roots, heartwood and
11 | sapwood), the autotrophic respiration, the production of litter, the plant mortality and the
12 | degradation of soil organic matter (CENTURY model; Parton et al., 1988). The hydrological
13 | processes for the soil reservoir rely on a double bucket scheme (Ducoudré et al., 1993). The
14 | link between the water and carbon modules is via photosynthesis, which is based on the leaf-
15 | scale equations of Farquhar et al. (1980) for C3 plants, and Collatz et al. (1992) for C4 plants,
16 | that are then integrated over the canopy by assuming an exponential attenuation of light. The
17 | FAPAR by each layer of the canopy is calculated from the leaf area index (LAI) following a
18 | Beer-Lambert extinction law (Bacour et al., 2015).

19 | ORCHIDEE uses the concept of the plant functional type (PFT) to describe the vegetation
20 | distribution, with 13 PFTs (including bare soil) that can co-exist in each grid cell. Except for
21 | the phenology (see a recent description in MacBean et al., 2015), the equations governing the
22 | different processes are generic, but with specific parameter values for each PFT. Detailed
23 | descriptions of model equations can be found in numerous publications (see for instance
24 | Krinner et al., 2005). ORCHIDEE can be run at either global scale on a grid, or at site-level
25 | using point-scale surface meteorological forcing variables. It is the land surface component of
26 | the Institut Pierre Simon Laplace (IPSL) Earth System Model, and the version that we used
27 | corresponds to CMIP5 simulations in the IPCC 5th Assessment Report (Dufresne et al., 2013).
28 | However, in this study the model is run offline using the ERA-Interim 3-hourly near surface
29 | meteorological forcing fields (Dee et al., 2011) aggregated at the spatial resolution of the
30 | atmospheric transport model for the global simulations (2.5° x 3.75°; see § 2.3.2). However,
31 | when we assimilate in situ flux data in the second step, we force the model with the gap-filled

Philippe Peylin 5/7/16 00:08

Mis en forme: Police :12 pt

Philippe Peylin 5/7/16 00:08

Mis en forme: Police :12 pt

Philippe Peylin 5/7/16 00:08

Mis en forme: Police :12 pt

Philippe Peylin 5/7/16 00:08

Mis en forme: Police :12 pt

Philippe Peylin 10/6/16 19:43

Supprimé: ,

1 half-hourly meteorological data measured at each site. The global PFT map was derived from
2 the high-resolution IGBP AVHRR land data set (Vérant et al., 2004). The carbon pools are
3 brought to equilibrium (spin-up procedure) for both site and global scale simulations by
4 cycling the available meteorological forcing over several millennia, to ensure that the long-
5 term net carbon flux is close to zero. For the global simulation in [the](#) third step, we spun-up
6 the model recycling the 1989-1998 meteorology and then used a transient simulation from
7 1990 to 2001 with changing climate (ERA-Interim) and increasing CO₂, before starting the
8 optimization with atmospheric data over 2002-2004. For the site simulations (i.e., the
9 assimilation of flux data) we recycled the available in situ meteorological forcing to spin-up
10 the model, with present day CO₂.

11 2.3.2 LMDz model

12 The transport model used in this study is version 3 of the General Circulation Model (GCM),
13 LMDz (Hourdin and Armengaud, 1999) with a horizontal resolution of 3.75° (longitude) x
14 2.5° (latitude) and 19 sigma-pressure layers up to 3 hPa. The calculated winds (u and v) are
15 relaxed to the ECMWF ERA-40 meteorological data (Uppala et al. 2005) with a relaxation
16 time of 2.5h (guiding) in order to realistically account for large-scale advection (Hourdin et
17 al., 2000). Deep convection is parameterized according to the scheme of Tiedtke (1989) and
18 the turbulent mixing in the planetary boundary layer is based on a local second-order closure
19 formalism. The LMDz GCM model has been widely used to model climate (IPCC, 2007,
20 2013) and its derived transport model has been used for the simulation of chemistry of gas
21 and particles and greenhouse gases distributions (Hauglustaine et al., 2004; Folberth et al.,
22 2005; Bousquet et al. 2005, 2006; Rivier et al., 2006). For this study, we used pre-calculated
23 transport fields, as described in Peylin et al. (2005), that correspond to the sensitivity of
24 concentration at each atmospheric site and each month to the surface flux of each model grid-
25 cell for each day (often called influence functions). The sensitivities (using inter-annual
26 winds) were calculated with the “retro-transport” formulation implemented in the LMDz
27 transport model (Hourdin et al. 2006). This approach decreases the computing time of the
28 optimization compared to the use of the full forward LMDz model at each iteration, as the
29 transport is replaced by a matrix multiplication with the vector of surface fluxes. Note that the
30 initial 3D state of the atmospheric concentrations was be defined from Chevallier et al. (2010)

1 2.3.3 Parameters optimized

2 The optimized parameters are described in Table 1, and their prior values, uncertainty and
3 range are given in Table 2. In the most recent studies using ORCHIDAS at site scales a large
4 set of ORCHIDEE parameters has been optimized (Kuppel et al., 2014; Santaren et al., 2014;
5 Bacour et al., 2015). In this study a smaller set was chosen, based on a Morris sensitivity
6 analysis (Morris, 1991; results not shown) that determines the sensitivity of the NEE and LE
7 to all model parameters at various FLUXNET sites (for each PFT), in order to reduce the
8 computational cost of the global optimization in step 3 (see §2.5). We considered 9 PFT-
9 dependent and 4 “global” (i.e. non PFT-dependent) parameters that control mostly the fast
10 carbon processes (diurnal to seasonal). In addition, we introduced a new parameter, K_{soilC} , to
11 scale the initial values (after spin-up) of the modeled slow and passive soil carbon pools, in
12 order to take account of all the historical effects not accounted for in the model that would
13 result in a disequilibrium of these pools in reality. For the site-specific optimizations with
14 FLUXNET data, we have one $K_{soilC,site}$ parameter per site. For the global scale optimization
15 step, we used 30 $K_{soilC,reg}$ parameters corresponding to 30 regions potentially coherent for land
16 use and land management history as well as ecosystem and edaphic properties (see Fig. A2).
17 The initial soil carbon pools of all pixels within each region were thus scaled by the same
18 value. The prior value for all K_{soilC} parameters was set to one, i.e. the default state of soil
19 carbon pools is assumed to be in equilibrium.

20 Overall (including all PFT-dependent parameters), we optimize 16 parameters related to
21 phenology, 36 to photosynthesis, 3 to respiration, 1 to the energy budget, 78 soil C pool
22 scalars (one for each FLUXNET site), and 30 regional soil C pool scalars for the global
23 simulations – a total of 184 parameters (16, 134 and 86 in step 1, 2 and 3, respectively). Note
24 that the soil C pool multipliers at the FLUXNET sites are independent from the regional C
25 pool multipliers, as the history of soil carbon over large eco-regions of several millions square
26 kilometers is rather heterogeneous (as it is mainly related to previous land use changes), and
27 most likely, the FLUXNET sites are not representative of larger regions in terms of the soil
28 carbon disequilibrium. The prior standard deviation for each parameter is equal to 40% of the
29 parameter range (lower and higher boundaries) prescribed for each parameter following
30 Kuppel et al. (2012). The parameter ranges were specified following expert judgment of their
31 meaning in the ORCHIDEE equations and based on literature reviews or databases (such as
32 TRY, Kattge et al., 2011).

Philippe Peylin 11/6/16 16:31

Supprimé: .

Philippe Peylin 11/6/16 16:31

Supprimé: thus the

1 2.4 System description: a step-wise approach

2 2.4.1 Stepwise assimilation of three data streams

3 The ORCHIDAS system relies on a stepwise assimilation of the three data streams described
4 in section 2.2. Figure 2 illustrates the flow of information in this sequential approach:

5 **Step 1 – Assimilation of MODIS-NDVI:** Four parameters related to the seasonal cycle of the
6 vegetation (phenology) are optimized for the temperate and boreal deciduous PFTs (TeBD,
7 BoND, BoBD and NC3 – see caption of Table 2). These four deciduous PFTs alone are
8 considered in step 1 in this ORCHIDAS version because the tropical deciduous phenology
9 modules in ORCHIDEE require further modifications to improve the functions that control
10 leaf growth and fall in response to water availability (MacBean et al., 2015). Evergreen PFTs
11 were also not considered, as there are no phenology modules related to these PFTs in the
12 model. The procedure is similar to that described in detail in MacBean et al. (2015) and
13 therefore only briefly recalled here. A simple linear relationship between the modeled
14 Fraction of Absorbed Photosynthetically Active Radiation (FAPAR) and MODIS-NDVI
15 observations is assumed, based on studies such as Knyazikhin et al. (1998). Given that
16 considerable discrepancies exist between so-called “high-level” satellite products such as LAI
17 or fAPAR when considering their magnitude (D’Odorico et al., 2014), we thus only use the
18 temporal information in the NDVI observations and normalized both the model FAPAR
19 output and the NDVI observations to their 5th and 95th percentiles (following Bacour et al.
20 (2015)). The model was run for fifteen randomly selected grid cells for each of the four PFTs
21 using the ERA-Interim meteorological forcing. Only grid cells that included vegetation
22 fraction of greater than 60% for the PFT optimized were considered. We selected a set of grid
23 points instead of the whole grid to substantially decrease the computing time; but the
24 remaining points are used for the evaluation of the optimized model. The fifteen sites for each
25 PFT were included in one optimization for each PFT following a multi-site approach, in
26 which all observations are used simultaneously to optimize the model parameters. The
27 optimized parameters are described in Table 1. They correspond to a scalar on the growing
28 degree days (GDD) threshold for the start of the vegetation ($K_{pheno,crit}$), a parameter controlling
29 the use of carbohydrate reserve during the start of leaf growth ($K_{lai,happy}$), a temperature
30 threshold for the onset of leaf senescence (CT_{senes}) and the critical age for leaves ($L_{agecrit}$).

Philippe Peylin 3/6/16 11:37

Supprimé: the

Philippe Peylin 11/6/16 08:28

Supprimé: Following Bacour et al. (2015), we use only the temporal information in the NDVI observations and not the actual values,

Philippe Peylin 11/6/16 08:26

Supprimé:

Philippe Peylin 11/6/16 08:26

Supprimé: and

Philippe Peylin 11/6/16 08:26

Supprimé: we

1 **Step 2 – Assimilation of FLUXNET data:** Mean daily NEE and LE flux measurements for 78
2 sites, including up to 10 years worth of data for each site, are used to optimize a set of model
3 parameters controlling the fast carbon and water processes (photosynthesis, respiration,
4 phenology – see Table 1). The site selection and the choice of a daily time step are described
5 in more details in Kuppel et al. (2014). These sites cover 7 of the PFTs in ORCHIDEE (see
6 Table 2). The posterior parameter values of the four phenology parameters derived in step 1,
7 and their associated uncertainties, are input as prior information in step 2. For the additional
8 parameters, the default ORCHIDEE values are used for the prior and the uncertainties are set
9 as described in §2.3.3. A multi-site optimization is performed for each PFT independently as
10 in step 1. Global parameters, i.e. those that are not PFT-dependent, were optimized for each
11 PFT and the mean across all PFTs was then calculated to define the prior parameter vector in
12 step 3 of the assimilation with atmospheric CO₂ data (at global scale). Such an approach was
13 chosen to allow us to optimize all PFTs in parallel and therefore to simplify the assimilation
14 process.

15 **Step 3 – Assimilation of atmospheric CO₂ concentrations:** We use monthly mean CO₂
16 concentrations from 53 surface stations over three years (2002-2004) to provide a large-scale
17 constraint to the land surface fluxes (i.e. to match the global CO₂ growth rate, mean seasonal
18 cycle and its latitudinal variation, as well as the spatial gradients between stations). We use
19 the LMDz atmospheric transport model (see §2.3.2) to assimilate these observations. The set
20 of parameters optimized in step 2 are included in step 3, except for the albedo scaling
21 parameter ($K_{albedo,veg}$), as the net carbon fluxes are only weakly sensitive to that parameter. We
22 used the posterior parameter distributions from step 2 (parameter optimal values and
23 associated uncertainties) as prior information for step 3, and expanded the parameter vector to
24 include the 30 K_{soilC} parameters that scale the initial soil carbon pools for large “spatially-
25 coherent regions” (see §2.1.2 and Fig. A2). The air-sea fluxes and fossil fuel and biomass
26 burning emissions are also accounted for (but not optimized) in this final step, in order to
27 close the global carbon budget within the atmospheric transport model (see §2.5).

28 2.4.2 Optimization procedure (for all steps):

29 In each step the statistically optimal parameter values are derived with an optimization
30 procedure following the principle of the 4-D variational assimilation systems (developed for
31 numerical weather prediction), using a tangent linear operator (and finite differences for a few
32 parameters, Bacour et al. 2015). Assuming that the errors associated with the parameters, the

1 observations and the model outputs follow Gaussian distributions, the optimal parameter set
2 corresponds to the minimum of a cost function, $J(\mathbf{x})$, that measures the mismatch between i)
3 the observations (\mathbf{y}) and the corresponding model outputs, $H(\mathbf{x})$, (where H is the model
4 operator), and ii) the a priori (\mathbf{x}_b) and optimized parameters (\mathbf{x}), weighted by their error
5 covariance matrices (Tarantola, 1987; [Chapter 4](#)):

$$6 \quad J(\mathbf{x}) = \frac{1}{2} \left[(H(\mathbf{x}) - \mathbf{y})^T \mathbf{R}^{-1} (H(\mathbf{x}) - \mathbf{y}) + (\mathbf{x} - \mathbf{x}_b)^T \mathbf{B}^{-1} (\mathbf{x} - \mathbf{x}_b) \right] \quad (1)$$

7 \mathbf{R} represents the error variance/covariance matrix associated with the observations and \mathbf{B} the
8 parameter prior error variance/covariance matrix. At each step a different cost function is
9 defined with the observations and parameters related to that step (see Fig. 2). \mathbf{R} includes the
10 errors on the measurements, the model structure and the meteorological forcing. Model errors
11 are rather difficult to assess and may be much larger than the measurement error itself.
12 Therefore we chose to focus on the structural error and defined the variances in \mathbf{R} as the mean
13 squared difference between the prior model and the observations for both step 1 and step 2
14 (see Kuppel et al. 2013). For simplicity we assumed that the observation error covariances
15 were independent between the different observations and therefore we kept \mathbf{R} diagonal (off-
16 diagonal terms set to zero), given the rapid decline of the model error auto-correlation beyond
17 one day (Kuppel et al., 2013). For step 3 we used a different approach, given the large bias in
18 the model a priori concentrations, and therefore followed the methodology of Peylin et al.
19 (2005) based on the observed and modeled temporal concentration variability at each site.
20 Overall, data uncertainties in the optimization procedure are between 0.1 and 0.45 for NDVI
21 (step 1), around 3-6 $\text{gCm}^{-2}\text{d}^{-1}$ for daily NEE, and 15-30 Wm^{-2} for daily LE (step 2) and
22 between 0.1 ppm at remote oceanic stations and 4 ppm at continental sites (step 3).

23 The determination of the optimal parameter vector that minimizes $J(\mathbf{x})$ is performed by
24 successive calls to a “gradient-descent” minimization algorithm L-BFGS-B (Byrd et al.
25 1995), which is specifically dedicated to solving large nonlinear optimization problems that
26 are subject to simple bounds on the parameter values. In order to find the minimum of $J(\mathbf{x})$ the
27 algorithm requires the gradient of $J(\mathbf{x})$ (Jacobian) with respect to the ORCHIDEE parameters.
28 L-BFGS-B explores each parameter space simultaneously along the gradient of the cost
29 function, and uses an approximation of the Hessian (second derivative) of $J(\mathbf{x})$, which is
30 updated at each iteration, to define the size of the step at each iteration.

Philippe Peylin 11/6/16 00:11

Supprimé: Eq. (1)

Philippe Peylin 11/6/16 00:11

Supprimé:)

1 For step 1 and step 2, the model “ H ” simply corresponds to the land surface model: $H = S$,
2 with $S(x)$ representing the surface fluxes from the ORCHIDEE model using the parameter
3 vector, x . The gradients $dJ(x)/dx$ are calculated from the tangent linear model of ORCHIDEE
4 that was automatically generated by the numerical Transformation of Algorithms in Fortran
5 (www.fastopt.de), except for two parameters linked to the model phenology for which the
6 threshold functions prevent the use of a linear approximation. A finite difference approach
7 was used for these parameters [in order to define a mean derivative at any point](#).

8 For step 3, the model “ H ” corresponds to the composition of the land surface model with the
9 transport model: $H = T \circ S$ (see Kaminski et al. (2002) for details), with T representing the
10 LMDz transport model. T is a linear operator for a non-reactive species: $T(S(x)) = \mathbf{T} \cdot S(x)$,
11 with \mathbf{T} a matrix representation of the transport operator. It corresponds to the sensitivity of
12 CO_2 concentrations at each site and for each month to the daily surface flux of each model
13 grid-cell. It is then combined with the ORCHIDEE surface fluxes ($S(x)$) through a matrix
14 multiplication to derive $H(x)$. \mathbf{T} has been pre-calculated for all atmospheric stations in order
15 to save computing time during the iterative optimization process (see §2.3.2). For simplicity
16 we use monthly mean values for both the fluxes $S(x)$ and the transport sensitivities (\mathbf{T}) in the
17 computation of the gradients $dJ(x)/dx$.

18 For improved minimization efficiency, the inversion is preconditioned (following Chevallier
19 et al., 2005), which means that L-BFGS-B is fed with the control variable $\mathbf{x}' = \mathbf{B}^{-1/2}(\mathbf{x} -$
20 $\mathbf{x}_b)$, rather than with \mathbf{x} , as this homogenizes the range of variation of the optimized
21 parameters.

22 2.4.3 Error estimation

23 The posterior parameter error covariance matrix, \mathbf{A} , can be approximated to the inverse
24 Hessian of the cost function, using the linearity assumption at the minimum of $J(\mathbf{x})$. It can be
25 derived with the Jacobian of the model at the end of the minimization (i.e. the last iteration),
26 \mathbf{H}_∞ , following Tarantola (1987):

$$27 \quad \mathbf{A} = [\mathbf{H}_\infty^T \cdot \mathbf{R}^{-1} \cdot \mathbf{H}_\infty + \mathbf{B}^{-1}]^{-1} \quad (4)$$

28 Note that for step 3, $\mathbf{H}_\infty = \mathbf{T} \cdot \mathbf{S}_\infty$, where \mathbf{S}_∞ is the Jacobian of the ORCHIDEE model at the
29 last iteration. The posterior parameter error covariance, \mathbf{A} , can then be propagated into the

1 model state variable space (e.g. carbon fluxes and stocks), \mathbf{A}_{var} , given the following matrix
2 product (only used for the global fluxes in step 3):

$$3 \quad \mathbf{A}_{\text{var}} = \mathbf{S}_{\infty} \cdot \mathbf{A} \cdot \mathbf{S}_{\infty}^{\text{T}} \quad (5)$$

4 The square root of the diagonal elements of \mathbf{A}_{var} corresponds to the standard deviation, σ , of
5 carbon fluxes/stocks for each grid cell. In order to evaluate the knowledge improvement
6 brought by the assimilation, the uncertainty reduction between the prior (σ_{prior}) and posterior
7 (σ_{post}) is determined as $1 - (\sigma_{\text{post}} / \sigma_{\text{prior}})$.

8 **2.4.4 Additional processing steps**

9 In order to analyze the fit to the atmospheric CO₂ concentrations in terms of the trend and
10 seasonal cycle, we decomposed the observed and modeled time series by fitting the monthly
11 mean values with a function comprising a first order polynomial term and four harmonics,
12 and then filtered the residuals of that function in frequency space using a low pass filter
13 (cutoff frequency of 65 days), following Thoning et al. (1989). The polynomial term defines
14 the trend while the seasonal cycle corresponds to the harmonics plus the filtered residuals.
15 The amplitude of the seasonal cycle is then calculated as the difference between the monthly
16 mean maximum and minimum for year 2003 (middle year of the optimization period).
17 Finally, we define the Carbon Uptake Period (CUP) as the sum of the days when the values of
18 the seasonal cycle extracted from the CO₂ concentration time series are negative (a negative
19 convention being for CO₂ removed from the atmosphere).

20 **2.5 Prescribed emissions of carbon fluxes**

21 In this section we describe the other components of the carbon cycle (apart from the surface C
22 exchange with terrestrial vegetation) that are imposed in step 3 of the optimization process as
23 fixed fluxes.

24 **2.5.1 Ocean fluxes**

25 The ocean contributes to an uptake of about a quarter to a third of the anthropogenic
26 emissions with significant year-to-year variations (Sabine et al., 2004). For this version of the
27 ORCHIDAS, we developed a statistical model to estimate the spatial and temporal variations
28 (monthly) of the ocean surface CO₂ partial pressure ($p\text{CO}_2^{\text{SW}}$), and from that the air-sea CO₂
29 fluxes, using satellite and in-situ ocean measurements and model outputs. The air-sea CO₂

1 fluxes are primarily controlled by the ocean biogeochemistry, the horizontal transport and the
2 vertical mixing in the ocean and the atmospheric forcing (CO_2 partial pressure at the interface
3 to the water (pCO_2^{ATM}) and wind); they can be defined from the following equation:

$$4 \quad F_{CO_2} = K_{ex} \times (pCO_2^{SW} - pCO_2^{ATM}) \quad (6)$$

5 where K_{ex} stands for the exchange coefficient and F_{CO_2} the CO_2 flux from the sea surface
6 water to the atmosphere.

7 The computation of pCO_2^{SW} is performed using feedforward artificial neural networks, i.e., a
8 MultiLayer Perceptron (MLP; Rosenblatt 1958) that maps a set of spatio-temporal variables
9 (input) onto observed pCO_2^{SW} data. We use a two-step approach: the first step to derive a
10 monthly mean pCO_2^{SW} climatology and the second step to correct for the year to year
11 variations. The pCO_2^{SW} observations come from the Global Surface pCO_2 (Lamont-Doherty
12 Earth Observatory, LDEO) Database (Takahashi et al., 2009). The inputs are a series of
13 variables connected to the spatial and temporal evolution of pCO_2^{SW} : i) sea surface
14 temperature (SST), sea surface salinity (SSS) and mixed layer depth (MLD) as a proxy of the
15 physical processes (these fields come from a re-analysis of the NEMO-OPA ocean model
16 (Madec et al., 1998) with the assimilation of several satellite observations), ii) chlorophyll
17 content from SeaWiFS, as a proxy of the biogeochemistry (CHL), iii) spatial and temporal
18 coordinates (LAT, LON and MONTH) and the pCO_2^{SW} at previous time step (recursive
19 approach), i.e.:

$$20 \quad \{pCO_2^{SW}\}_m = MLP(\{SST, SSS, MLD, CHL\}_{(m-2, m-1, m)}, \{pCO_2^{SW}\}_{(m-2, m-1)}, LAT, LON) \quad (7)$$

21 with m the monthly index. The available data (20685 points) is divided into two parts: 75% is
22 used for the learning phase of the ANN and 25% for the validation phase. The overall
23 performance of the neural network for extrapolating the spatial and seasonal distribution of
24 pCO_2^{SW} is relatively good, with a spatio-temporal correlation coefficient between the
25 estimated pCO_2^{SW} and the independent observations of 0.80.

26 pCO_2^{ATM} at the surface are taken from a global simulation of atmospheric CO_2 concentrations
27 with optimized fluxes (Chevallier et al. 2010). K_{ex} is defined as the product of k , the gas
28 transfer velocity, taken from the Wanninkhof (1992) formulation using winds from ERA-
29 Interim, and s , the solubility of CO_2 , taken from the Weiss formulation (Weiss, 1974). The
30 system is further described in Roedenbeck et al. (2015). The global ocean sink is around 1.60
31 $PgC.yr^{-1}$ for the period 2002-2004 used in step 3. It is within the uncertainty range of the

1 Global Carbon Project estimates (Le Quéré et al., 2015) if we account for the pre-industrial
2 ocean outgazing flux included in our “delta pCO₂” approach. Its temporal evolution is
3 depicted in Fig. A1

4 2.5.2 Global fossil fuel and cement CO₂ emissions

5 We have used a recently developed CO₂ fossil fuel and cement emission product (see
6 <http://www.carbones.eu/wcmqs/>) that covers the period 1980 to 2009 at the spatial resolution
7 of 1° x 1° and hourly resolution. It is based on EDGAR v4.2 spatially distributed annual
8 emissions (Olivier et al., 2012) and time profiles developed by the University of Stuttgart
9 (<http://carbones.ier.uni-stuttgart.de/wms/impressum.html>). It was assumed that EDGAR
10 delivers the most up-to-date spatially distributed and sector specific emissions, based on
11 national emission statistics. [The IER \(Institut für Energiewirtschaft und Rationelle](#)
12 [Energieanwendung\)](#) further applied country and sector specific time profiles, taking into
13 account monthly, daily, and hourly variations depending on the sector. The derivation of the
14 time profiles relies on different data sets (e.g. Eurostat, ENSTO-E
15 (<https://www.entsoe.eu/about-entso-e/Pages/default.aspx>), UN monthly bulletin) as well as
16 correlations between recorded emissions and climate variables. Currently, the temporal
17 profiles are derived mostly from data sets over Europe that were extrapolated using
18 information on climate zone, average monthly temperature for the seasonal cycles and
19 similarity in socio-economic parameters like population and Gross Domestic Product (GDP).
20 The annual mean emission for the period 2002-2004 is 7.14 PgC.yr⁻¹.

21 2.5.3 Fire emissions:

22 Fire emissions data from the Global Fire Data (GFEDv3 –
23 <http://www.globalfiredata.org/Data/index.html>) are prescribed in the ORCHIDAS [\(except](#)
24 [during the model spin-up\)](#). The GFEDv3 data are broken-down into 6 sectors (deforestation,
25 peat fires, savanna fires, agriculture, forest fires, and woodland) that are further grouped into
26 3 main types. We generated fluxes of CO₂ relevant for typical "burning - regrowth" processes,
27 as detailed in Appendix A2. The first type corresponds to deforestation and peat fires with
28 carbon permanently lost to the atmosphere, the second to agriculture and savannah fires which
29 are assumed to be compensated by a sink during the regrowth period (i.e. with zero annual net
30 emission for each pixel) and the third to woodland and burnt forests which are assumed to be
31 at steady state for a given region (10 sub-continental scale regions) over the period covered by

1 GFEDv2 (i.e. regrowth of nearby forest compensates for the burned forest derived in GFED).
2 The sum of these three components leads to the global flux, with a gross emission around 2.1
3 PgC.yr⁻¹ and a net emission after regrowth of only 1.1 PgC.yr⁻¹ (Fig. A2 in Appendix) that is
4 prescribed to the ORCHIDAS over the period 2002-2004.

5

6 **3 Results**

7 **3.1 Model fit to the data**

8 **3.1.1 Step 1: assimilation of MODIS NDVI data**

9 The optimization in Step 1 resulted in an improved fit to the MODIS NDVI observations for
10 the four PFTs considered (TeBD, BoND, BoBD, NC3, see §2.4) as seen in Fig. 4, which
11 shows the mean seasonal cycle across the 2000-2008 period for all sites for each PFT. The
12 most prominent change after the optimization was a substantially shorter growing season for
13 all PFTs due to an earlier start of leaf senescence. This was caused by both a lower critical
14 leaf age ($L_{agecrit}$) and a higher temperature threshold for senescence ($C_{T_{senes}}$) (see Fig. 9). The
15 impact on the start of leaf growth was less dramatic but important nonetheless, with a shift to
16 a later start of leaf growth as a result of an increase in the $K_{pheno,crit}$ parameter which acts as a
17 scalar on the threshold of Growing Degree Days (GDD) used to trigger leaf onset (see
18 Appendix A in MacBean et al., 2015). Overall, a mean reduction in RMSE of 23, 17, 58 and
19 19% was achieved for TeBD, BoBD, BoND trees and NC3 grasses respectively, with the
20 greatest improvement for BoND trees. The mean correlation between the normalized MODIS-
21 NDVI and modeled FAPAR time series over the 2000 – 2008 period increased for TeBD and
22 BoND trees and NC3 grasses (prior and posterior of 0.9 to 0.93, 0.42 to 0.91 and 0.6 to 0.66,
23 respectively). The prior correlation of 0.55 remained similar after the assimilation for BoBD
24 trees.

25 Following the improvement at the sites selected for the optimization, we evaluated the impact
26 for each PFT at the global scale using the global median correlation between the MODIS-
27 NDVI and the model FAPAR time series (from all pixels where the fraction of a given PFT is
28 above 60%, see Maignan et al. 2011). The global correlation increased for BoND trees and
29 NC3 grasses from 0.36 to 0.91 and 0.53 to 0.59 (prior to posterior), respectively. It remains
30 stable for BoBD (0.54) or slightly increased for TeBD (0.88 to 0.89).

Philippe Peylin 3/6/16 16:40

Supprimé: 8

1 3.1.2 Step 2: assimilation of FLUXNET data

2 The optimization in Step 2 brings an improvement to the simulated NEE and LE for all seven
3 PFTs considered, with Fig. 5 showing the corresponding PFT-averaged mean NEE seasonal
4 cycles (mean across all sites/years). NEE is overestimated by the prior model for all PFTs on
5 average. This is partly due to the model spin-up procedure, which brings each simulated site
6 to a near equilibrium state with a mean NEE close to zero (i.e. no net carbon sink, see §2.1.1).
7 This bias is significantly corrected by the optimization to match the observed carbon uptake at
8 most sites, notably via the scaling of the initial soil carbon pool content at each site
9 (parameters $K_{soilC,site}$; Table 1) which thus significantly reduces the ecosystem respiration
10 (Kuppel et al., 2014). Overall, the largest reductions of model-data RMSE are found in
11 temperate forests (TeNE, TeBE and TeBD), where the RMSE decreased by more than 25%
12 compared with the prior model. The improvements are less significant for the other PFTs,
13 with RMSE reductions between 10 and 18%.

14 In addition, the optimization increases the NEE seasonal amplitude in temperate evergreen
15 forests (TeNE and TeBE) and temperate broadleaf deciduous forests (TeBD), and reduces the
16 amplitude for boreal needle leaf forest (BoNE) and natural C3 grasses (NC3), in agreement
17 with the observations (except for BoNE where the amplitude decrease is too large). Despite
18 the better model-data agreement for evergreen broadleaf forests (TrBE and TeBE), the
19 optimized model still fails to catch some seasonal features such as a persistent carbon uptake
20 (i.e. negative NEE) in the dry season for the tropical regions (TrBE) and nearly-null carbon
21 exchange in the first months of the year for temperate regions (TeBE). These results are
22 discussed further in Kuppel et al. (2014), who used a similar optimization set-up with a
23 slightly different parameter set – see §2.3.3. Similar improvements, although of smaller
24 amplitude, occur for the latent heat fluxes (not shown).

25 3.1.3 Step 3: assimilation of atmospheric CO₂ data

26 The final optimization step with the atmospheric CO₂ concentrations provides a large
27 improvement of the fit to the observed concentrations at most stations. The cost function J
28 was reduced through the minimization by a factor of 5.7 within 37 iterations.

29 Figure 6 illustrates the simulated concentrations for four stations (representative of different
30 conditions) with the standard prior parameter vector (used in step 1), the posterior vector from
31 step 2 (used as prior in step 3) and the posterior vector from this last step. The improvement

1 in the fit to the observations can be quantified with the reduction in RMSE (from the prior to
2 the posterior of step 3) - the largest reduction is at the South Pole station (73%) and is on
3 average around 25% across all sites. Note that for a few stations the fit is slightly degraded
4 (up to 10%) except for one Pacific site (regular ship measurements around the equator,
5 POCN00) for which there is a 40% degradation, possibly due to small biases in the simulation
6 of the ITCZ position in LMDz. When calculated with respect to the standard prior (used in
7 step 1) the RMSE decrease is slightly larger on average, especially for the northern mid to
8 high latitude stations. For these stations the optimization performed in step 2 with FLUXNET
9 data led to a significant improvement of the mean seasonal cycle amplitude of the
10 atmospheric CO₂ data, as discussed in Kuppel et al. (2014).

11 We then investigated the fit to the observed CO₂ concentrations in terms of the mean seasonal
12 cycle and trend (see section 2.4.4). With only three years of data the mean trend is more
13 difficult to define as it varies between stations; however, the optimization in step 3 increases
14 the net land carbon sink in order to match the observed trend at most stations (as expected). If
15 we take the Mauna Loa and South Pole stations that are representative of an integration of the
16 fluxes at hemispheric scales, the prior CO₂ trend of 2.8 and 2.9 ppm.yr⁻¹ respectively, is
17 reduced to 2.1 and 2.2 ppm.yr⁻¹ close to the observations (2.1 ppm.yr⁻¹ for both). The left
18 panel of Fig. 7 illustrates changes in the amplitude of the simulated seasonal cycle at each
19 station (see definition in §2.4.4). The values correspond to relative changes between the prior
20 (of step 3) and posterior of the absolute difference between observed and modeled amplitude
21 ($|\Delta A_{poste}| - |\Delta A_{prior}| / |\Delta A_{prior}|$). They reveal an improvement in the seasonal cycle
22 amplitude at nearly all stations of the southern hemisphere ($\approx 40\%$ improvement) and at the
23 majority of the northern hemisphere stations ($\approx 15\%$). A few stations in north East Asia (3)
24 and northwest America (4) show a small degradation of the amplitude ($\approx 15\%$). The right
25 panel of Fig. 7 displays the changes of the Carbon Uptake Period (CUP, see §2.4.4) expressed
26 in terms of relative changes between prior and posterior of the absolute values of model-data
27 differences, as for the amplitude. Most stations reveal an improvement of the CUP of around
28 20%, which is slightly lower than the improvement for the seasonal cycle amplitude.

29 Finally, we verified that the improvement is not only valid at the optimization sites but also at
30 independent atmospheric CO₂ stations (see section 2.2.3). On average the mean RMSE for the 24
31 additional sites is 10.5 ppm for the prior of step 1 (prior of ORCHIDEE), 2.8 ppm for the prior or step
32 3 (i.e. posterior of step 2) and 2.1 ppm for the posterior of step 3. The corresponding values for the 53
33 sites used for the optimization are 10.5, 2.45 and 1.8 ppm, respectively. The error reduction during

1 | [step 3 is thus similar for both the assimilated and the validation data sets, further confirming that the](#)
2 | [optimization provides a global improvement of the simulated carbon fluxes.](#)

3 | **3.2 Consistency of the step-wise optimization**

4 | The main issue with a step-wise data assimilation system (versus a simultaneous approach)
5 | concerns the potential degradation of the model – data fit for the different data streams that
6 | are assimilated in previous steps. We noted that CO₂ concentrations were already improved
7 | when NDVI and FLUXNET data are assimilated (see §3.1.3), but we need to check if the
8 | final parameter set from step 3 leads to a degradation of the fit to MODIS-NDVI (step 1) and
9 | to FLUXNET (step 2) data compared to the fit achieved during the respective steps and, in the
10 | case of a significant degradation, if we still have an improvement for these data streams
11 | compared to the initial *a priori* fit.

12 | Figure 8 summarizes the performance of the model data fit for MODIS-NDVI and
13 | FLUXNET-NEE data streams for the prior and posterior of each step by evaluating the
14 | median RMSE between the model and the observations across all sites. The values are
15 | calculated for each PFT separately. In this section, we keep in mind the fact that we do not
16 | optimize the same PFTs with FLUXNET data and with MODIS-NDVI.

17 | **Consistency for MODIS-NDVI**

18 | First, we notice again the significant RMSE reduction between the prior and step 1, as
19 | discussed in section 3.1. The fit to MODIS-NDVI (normalized data) for step 2 and step 3
20 | shows only a significant degradation (increased RMSE) for temperate broadleaf deciduous
21 | forest (TeBD), which decreases the improvement achieved in step 1 (compared to the prior)
22 | by a factor of two. A marginal degradation for natural C3 grassland (NC3) is obtained after
23 | step 3: the RMSE increases slightly from 0.24 to 0.26, but is still lower than the prior value of
24 | 0.3. There is no degradation for boreal needleleaf deciduous trees (BoND), but a surprising
25 | small decrease of the RMSE (i.e. improvement in the model-data fit) for boreal broadleaf
26 | deciduous forests (BoBD; from 0.26 to 0.23). In this latter case, the use of additional
27 | parameters in steps 2 and 3 (see §2.4) allows further improvement of the fit between the
28 | normalized FAPAR and NDVI time series. On average the degradation of the fit to NDVI is
29 | thus very limited in step 2 and step 3, and in no case is the RMSE worse than the prior.

1 Consistency for FLUXNET data

2 Figure 8 again reveals the significant reduction of the RMSEs for NEE in step 2 compared to
3 the standard prior or to the posterior of step 1 for most PFTs, except BoNE. We see only
4 small degradations (increases) in RMSE between step 2 and step 3 for temperate needle leaf
5 evergreen forests (TeNE: from 1.06 to 1.13 $\text{gC.m}^2.\text{d}^{-1}$), temperate broadleaf evergreen forests
6 (TeBE: from 1.06 to 1.09 $\text{gC.m}^2.\text{d}^{-1}$), temperate broadleaf deciduous forests (TeBD: from 1.06
7 to 1.13 $\text{gC.m}^2.\text{d}^{-1}$) and boreal needle leaf evergreen forests (BoNE: from 0.59 to 0.60 $\text{gC.m}^2.\text{d}^{-1}$).
8 An interesting feature to notice is that the NEE RMSE increases from the prior to the
9 posterior of step 1 (i.e. before NEE has been used in the optimization in step 2). Using remote
10 sensing products of vegetation activity or “greenness” (e.g. NDVI) to calibrate the phenology
11 of ORCHIDEE thus does not always improve the simulated NEE, as they only provide a
12 strong constraint on the timing of the GPP and a weak constraint on the maximum GPP but no
13 constraint on the respiration fluxes. These reasons were discussed in Bacour et al. (2015) who
14 used the same LSM and assimilation system. Overall, the reduction of the improvement of the
15 model data fit to the NEE (step 3 versus step 2) is marginal (limited to a few percent), thus
16 further suggesting the consistency of our step-wise approach. Similar results are also obtained
17 for the latent heat flux (LE) (not shown).

Philippe Peylin 3/6/16 16:42

Supprimé: between

Philippe Peylin 16/5/16 18:24

Supprimé: the possible

Philippe Peylin 16/5/16 18:24

Supprimé: for which

18 3.3 Estimated parameter values

19 We now discuss the parameter values, focusing on the changes obtained through the
20 successive steps. Figure 9 presents the prior and posterior values for each parameter together
21 with their associated uncertainties (estimated through Eq. (4)) and the allowed range of
22 variation. Note that nine parameters are PFT-dependent while four are global (non PFT-
23 dependent). For the global non PFT-dependent parameters included in the step 2 optimization,
24 we took the mean value and error-variance (see §2.4) as the prior for step 3. Note finally that
25 the parameters linked to the initial soil carbon pools ($K_{soilC,site}$, $K_{soilC,reg}$) are not shown in Fig.
26 9 as they are too numerous (though see Fig. A2 for the regional values).

27 If we first consider the phenology parameters optimized in step 1 ($K_{lai,happy}$, $K_{pheno,crit}$, $L_{age,crit}$,
28 $C_{T,senes}$; see Table 1) we see that for most PFTs they do not change significantly between step
29 1 and step 3, although they differ significantly from the prior. There are few exceptions,
30 including $K_{pheno,crit}$ (the threshold for the start of the growing season) for Boreal Needleleaf
31 deciduous forests and $K_{lai,happy}$ (level of carbohydrate use) for temperate and boreal broadleaf

1 deciduous forests (TeBD, BoBD). Note that a few phenology parameters hit one of the
2 physical bounds, which may indicate model structural errors or model parameter equifinality.
3 For most phenology parameters, the uncertainties are strongly reduced during their first
4 optimization (step 1), except for a few cases like $C_{T,senes}$ for C3 grassland. Note finally that a
5 more in depth spatio-temporal validation demonstrated the generality of the optimized
6 phenology parameters across multiple sites (for further details see MacBean et al., 2015).

7 For the photosynthesis parameters (V_{max} , $G_{s,slope}$, C_{Top} , SLA , f_{stress} ; see Table 1), we find a
8 similar result with little changes between step 2 and step 3, but still a significant departure
9 from the prior values. Most parameters are well constrained by the inversion, with posterior
10 uncertainties that are greatly reduced compared to the prior, except for Tropical broadleaf
11 rain-green forest (TrBR) and Boreal needle-leaf deciduous forest (BoND) for which there is
12 nearly no constraint on $G_{s,slope}$ and f_{stress} (see Table 1).

13 The non-PFT dependent respiration-related parameters ($HR_{H,c}$, Q_{10} , MR_b) mostly change in
14 step 2 and only slightly in step 3 (with an additional reduction of the error) in order to fit the
15 large-scale constraint provided by the atmospheric observations. The values of the scalar of
16 the initial soil carbon pools size for the FLUXNET site optimizations ($K_{soilC,site}$, one parameter
17 per site, not shown) were largely reduced on average, in order to decrease the heterotrophic
18 respiration (see Kuppel et al. (2014) for additional discussion). In step 3 the same scalars that
19 were defined for an ensemble of large regions ($K_{soilC,reg}$) have decreased in the southern
20 hemisphere (less than 10%; see Fig. A2 in Appendix A3) and slightly increased in the
21 northern hemisphere (around 1%), to achieve a better match to the atmospheric CO₂ growth
22 rate and north-south gradient. Importantly, we notice that for step 3, the fit to the atmospheric
23 CO₂ concentrations (especially to the trend) is achieved mainly by small changes in $K_{soilC,reg}$
24 and in few other respiration-related parameters. Note finally that the parameter controlling the
25 albedo ($K_{albedo,veg}$), modified with the FLUXNET observations only (see §2.4), is not well
26 constrained by the optimization (only a small reduction in uncertainty). Overall, most
27 parameters appear to be well constrained when first optimized, with only small changes in the
28 following steps. This suggests that the targeting of different parameter subspaces in the
29 various optimisation steps was well-chosen.

1 **3.4 Estimated carbon fluxes and uncertainties**

2 The main objective of a carbon cycle data assimilation procedure is to improve the simulated
3 land surface net and gross carbon fluxes as well as the simulated carbon stocks for both
4 present and future conditions. Given the focus of the paper, i.e. to describe the potential of a
5 step-wise global carbon cycle data assimilation system, we only discuss a few large-scale
6 features of the optimized annual net and gross carbon fluxes, as well as one of the carbon
7 stock variables (forest above-ground biomass). We thus do not discuss the inter-annual flux
8 variability.

9 **Large-scale annual mean net fluxes**

10 The mean annual carbon fluxes (NEE) for the globe, northern extra tropics, tropics, and
11 southern extra tropics are reported in Fig. 10 for the 2000-2009 decade for the prior and
12 posterior model simulations for all steps together with one other estimate of the land surface
13 residual from the Global Carbon Project (GCP, Le Quéré et al, 2015) over the same decade.
14 The prior NEE indicates a total sink of 0.5 PgC.yr^{-1} over this period, from both the northern
15 and tropical regions. Such a prior sink is due to the increase of atmospheric CO_2 during the
16 transient simulation following the spin-up (1990-2009, see section 2.3.1) and climate
17 variability. Changes from the prior are rather small in step 1 (assimilation of MODIS NDVI)
18 with an increase of the northern sink by 0.12 PgC.yr^{-1} and a decrease of the tropical sink by
19 0.05 PgC.yr^{-1} (Fig. 10). Step 2 (assimilation of FLUXNET data) does not significantly change
20 the net C sink from step 1, with only a small increase in the tropical sink by 0.1 PgC.yr^{-1} . The
21 assimilation of atmospheric CO_2 data in step 3 provides a large-scale constraint, as already
22 discussed, and increases the total land sink to 2.2 PgC.yr^{-1} , a value in much closer agreement
23 with the estimate by the GCP. A larger tropical NEE uptake is responsible for the large
24 increase of the terrestrial biosphere C sink (from 0.3 PgC.yr^{-1} in step 2 to 1.7 PgC.yr^{-1}) while
25 the sink in the north increases by less than 0.1 PgC.yr^{-1} . The comparison with the GCP
26 number should be taken with caution. The ORCHIDAS estimated sink include all effects
27 (natural and anthropogenic), since that we used atmospheric CO_2 as a global constraint. Thus
28 the optimized parameters must account for any missing processes like nitrogen limitation or a
29 proper description of agricultural processes and management. However, the GCP number is
30 only for the anthropogenic uptake, excluding the pre-industrial sink due for instance to river
31 export of carbon (around 0.45 PgC.yr^{-1} ; Regnier et al. 2013).

1 Spatial distribution of the annual mean net flux

2 Figure 11 shows the spatial distribution of NEE averaged over 2002-2004 for the standard
3 prior and posterior after step 3. The large tropical net land carbon sink that is inferred in step
4 3 is mainly explained by an increase of the carbon uptake for the tropical forests of the
5 Amazon basin and equatorial Africa, as well as a decrease of the carbon release on the
6 southern edge of the Amazon basin (tropical rain-green forests and grasses). In the northern
7 mid-high latitudes only smaller regional changes from the prior occur. For Europe, most of
8 north Asia and Canada, the strength of the C sink slightly decreased from the prior (up to 30
9 $\text{gC.m}^2.\text{yr}^{-1}$), while for central USA the strength of C source slightly decreased. If we now
10 consider the uncertainties on the net annual carbon flux that arise from the parameter
11 uncertainty (second row of Fig. 10; Eq. (5)) we observe a very large reduction (compared to
12 the prior) in the monthly flux uncertainty (averaged over the three years used in step 3) over
13 tropical forests. It is reduced by a factor four with initial values around $150 \text{ gC.m}^2.\text{y}^{-1}$ and
14 posterior values between 22 and $66 \text{ gC.m}^2.\text{y}^{-1}$. For mid-to-high latitude boreal ecosystems, the
15 uncertainty reduction is smaller, but the posterior errors are slightly lower than over the
16 tropics, between 18 and $55 \text{ gC.m}^2.\text{y}^{-1}$.

17 Large-scale annual mean Gross Primary Production (GPP)

18 For the GPP the relative changes from the prior are smaller than for the NEE (Fig. 10b). The
19 mean annual total GPP is 172, 155, 156, and 157 PgC.yr^{-1} for the prior and posterior of step 1,
20 2 and 3, respectively. The small overall decrease (9%) brings the GPP slightly closer to the
21 estimate by Jung et al. (2011), around 120 PgC.yr^{-1} , based on a statistical Model Tree
22 Ensemble (MTE) that upscaled the in-situ flux measurements (resulting from the partition of
23 measured NEE into GPP and total ecosystem respiration). The decrease in GPP occurs mainly
24 in the northern hemisphere after step 1 (-10 PgC.yr^{-1}) following the decrease in V_{cmax} (Fig. 9)
25 while it remains relatively stable over the tropics across all steps. Note that i) the study of
26 Welp et al. (2011) suggests a GPP around 150 PgC.yr^{-1} , similar to our estimate, based on
27 measurements of $^{18}\text{O}/^{16}\text{O}$ ratio in atmospheric CO_2 and ii) Koffi et al. (2012) found optimized
28 GPP of 146 PgC.yr^{-1} from a CCDAS using the BETHY model.

29 Above-ground forest biomass

30 We analyze the impact of the optimization on the forest above-ground biomass at equilibrium
31 (i.e. after spin-up; see Fig. 12) as an example of the impact on model C stocks, and compare

Philippe Peylin 16/5/16 19:46

Supprimé: 169

Philippe Peylin 16/5/16 19:45

Supprimé: 160

Philippe Peylin 16/5/16 19:45

Supprimé: 4

Philippe Peylin 16/5/16 19:45

Supprimé: 6

Philippe Peylin 16/5/16 19:47

Supprimé: 8

1 the simulated values, for the same three latitude bands than above, to the estimate based on
2 field observations and remote sensing data. This product, which was produced in the
3 GEOCARBON project (and thus is referred to by the same name), integrates a pan-tropical
4 biomass map (Avitabile et al., 2015) with a boreal forest biomass product (Santoro et al.,
5 2015).

6 For the northern extra tropics, the prior above-ground C stock (~180 PgC) is reduced by the
7 optimization to 140 PgC, mainly through the decrease of the growing season length in step 1
8 with the assimilation of MODIS-NDVI. The significant decrease in GPP during step 1 (18 %)
9 led indeed to a similar decrease of the forest biomass (16%). Parameter changes through the
10 assimilation of FLUXNET and CO₂ data have a smaller impact (a change of less than 5 PgC).
11 These changes in the northern extra tropics bring the estimates by the ORCHIDEE model
12 closer to the satellite-based GEOCARBON product (~ 120 PgC).

13 For the tropics, while there is nearly no change with the assimilation of MODIS-NDVI in step
14 1, the use of FLUXNET data leads to a significant increase of the forest above ground
15 biomass (close to 25%). Such an increase does not correspond to an increase of the GPP (Fig.
16 10) but to changes in the autotrophic respiration parameter (MR_b) that lead to a decrease of
17 autotrophic respiration and an increase of NPP. The value does not change through step 3 and
18 remains significantly higher than the data-driven estimate. Note however that the lower value
19 in the GEOCARBON product could be partly due to the fact that we did not yet account for
20 land use effects in the CCDAS, such as deforestation in the Amazon.

21

22 **4 Discussion and conclusions**

23 In this paper we have described a first global Carbon Cycle Data Assimilation System that
24 assimilates three major carbon-cycle related data streams, namely MODIS-NDVI
25 observations of vegetation activity at 60 sites, FLUXNET NEE and LE measurements at more
26 than 70 sites, and atmospheric CO₂ concentrations at 53 surface stations over three years in
27 order to optimize the C cycle parameters of the ORCHIDEE process-based LSM
28 (ORCHIDEE-CCDAS). The study details the concept, the implementation and the main
29 results of a stepwise assimilation approach where the data streams have been assimilated in
30 three successive steps (including a propagation of the retrieved posterior parameter
31 distributions from one step to the next).

1 The assimilation of MODIS-NDVI (60 grid cell points, step 1) improved the phenology of
2 ORCHIDEE with a significant reduction of the growing season length and thus a direct
3 impact on the GPP. The results are similar to those presented in MacBean et al. (2015) who
4 describe the impact of such optimization on the global FAPAR simulations and the
5 improvement in the bias of the calculated leaf onset and senescence dates in more detail. The
6 optimization with FLUXNET data (78 sites, step 2) led to large improvements in the seasonal
7 cycle of the NEE and LE fluxes, constraining primarily the photosynthetic processes. Some
8 discrepancies remain due to site heterogeneity (i.e. different species and edaphic conditions)
9 that the model does not fully capture, and due to missing processes in the model (see Kuppel
10 et al. (2014) for a more thorough discussion). However, without the assimilation of
11 atmospheric CO₂ concentrations, the global (and continental) net carbon balance after step 2
12 was still clearly outside the admitted range (as reported by the GCP in Le Quéré et al. (2015),
13 which highlights the importance of assimilating a data stream such as this that provides
14 information at larger scales (constraining large scale respiration fluxes). The use of
15 atmospheric CO₂ concentration as an overall constraint in step 3 was technically challenging
16 as it required the coupling of ORCHIDEE with an atmospheric transport model in forward
17 and reverse mode (i.e. to compute the cost function and its gradients at each step of the
18 minimization process). As a result of the final step, we were able to fit the atmospheric CO₂
19 growth rate and thus to derive a land C sink compatible with current best estimates from the
20 GCP. The assimilation of CO₂ data also slightly changed the seasonality of the NEE, which
21 improved the fit to the atmospheric CO₂ seasonal cycle. Note that assimilating only CO₂ data
22 would lead to a similar global land C sink but with a different model parameter set not
23 compatible with the information provided by MODIS-NDVI and FLUXNET data.

24 The consistency of the stepwise approach has been evaluated with back-compatibility checks
25 after the final step (step 3: assimilation of atmospheric CO₂ concentration). The optimized
26 model with the final set of parameters does not degrade the fit to MODIS-NDVI and
27 FLUXNET data that were assimilated in the first two steps (only minor changes of the
28 RMSEs occur; see Fig. 8). This result has two important consequences. Most importantly it
29 suggests that current state of the art LSMs (at least ORCHIDEE) have reached a level of
30 development where consistent assimilation of multiple data streams is finally possible. This
31 overcomes the most important limitation noted by Rayner (2010) to the widespread use of
32 CCDAS systems. At a more technical level it suggests that stepwise assimilation is a valid
33 and feasible approach. Although we only carried the estimated parameter uncertainties from

1 | one step to the next (as a first more simple approach), and not the full error variance-
2 | covariance matrix, we were able to propagate enough information to maintain an optimal
3 | model-data fit after the last step for the three data streams, as confirmed with the back-
4 | compatibility checks. MacBean et al. (2016) provide a more specific analysis of this issue.
5 | However, not propagating the covariance terms may have a larger impact for the reduction of
6 | the inferred parameter uncertainties (see for instance the large parameter / flux error reduction
7 | in Fig. 9 / Fig. 11). The order of the different steps was dictated by the number of parameters
8 | we choose to expose to each data stream, from only a few phenology parameters for NDVI up
9 | to the largest set for atmospheric CO₂. Recall that under the fundamental theory the order of
10 | assimilation is unimportant. Testing whether our system meets this criterion is an important
11 | check on the robustness of the method but is not technically feasible with the full-blown
12 | system; it is currently being tested with some smaller models.

13 | Most of the optimized parameter values have significantly changed compared to their prior
14 | values, with a large error reduction for most (Fig. 9) that results in a strong constraint on the
15 | simulated fluxes (Fig. 11). In the last step, the assimilation of atmospheric CO₂ data mainly
16 | led to the optimization of respiration-related parameters, especially the regional soil carbon
17 | multipliers ($K_{soilC,reg}$). Note that this was also the case for the BETHY-CCDAS, as described
18 | in Rayner et al. (2005) (see their Table 2). This is linked to the difficult issue of representing
19 | the effects of historical changes in land cover and land management as well as soil texture
20 | effects on soil carbon dynamics, and the necessary choice of a standard spin-up procedure to
21 | account for these effects. Ideally one would need to perform the optimization of the model
22 | over a long historical period with LULCC and land management practices included and the
23 | optimization of related parameters. However, this is not currently feasible at global scale and
24 | uncertainties in the forcing would introduce as much difficulty as uncertainties in the initial
25 | condition. The adjustment of the initial C pool contents is thus a logical compromise and
26 | further investigations into the impact of the selected set-up (number of regions for $K_{soilC,reg}$,
27 | their associated uncertainties) on the C fluxes simulated in the future are needed. Note that a
28 | first improvement would be to include LULCC in the transient simulation (to define the initial
29 | state) before the assimilation period.

30 | Nonetheless, several limitations, inherent to the optimization of model parameters in a
31 | CCDAS, need to be called to mind when evaluating these results (see also Rayner et al.,
32 | 2010). First, the structure of the land surface model (i.e. how biogeochemical processes are

Philippe Peylin 11/6/16 16:39

Supprimé: (see

Philippe Peylin 11/6/16 16:39

Supprimé: for

Philippe Peylin 11/6/16 16:39

Supprimé:)

1 represented) is critical. Any missing/misrepresented processes may have a direct impact and
2 thus lead to biases in the selected parameters. Note that this limitation could be even more
3 severe when using atmospheric CO₂ measurements, as these data provide a direct constraint
4 on the overall net C exchange between the atmosphere and the vegetation, thus including all
5 processes. As an example, the model sensitivity to atmospheric CO₂ increase (e.g. through the
6 parameters V_{max} and $G_{s,slope}$) could be non optimal as the current model version does not
7 include explicit nitrogen and phosphorus limitations on photosynthesis. Second, the chosen
8 set of observations does not provide specific constraints on long term C processes such as tree
9 mortality, disturbance effects, or C allocation within a plant. For instance Fig. 12 illustrates
10 that the optimized model may still significantly overestimate tropical forest biomass. The
11 assimilation of above-ground biomass or soil carbon stock observations (i.e. site-level
12 measurements or regional estimates) should thus provide critical complementary information
13 (see [Bloom et al., 2016](#) and Thum et al., in revision for AFM). Additionally, uncertainties on
14 the other components of the carbon cycle, such as fossil fuel and biomass burning emissions
15 and ocean fluxes, can be also critical when using atmospheric CO₂ as a constraint. Finally,
16 one can mention new approaches based on remote sensing data to account for site level
17 differences in productivity potential due to edaphic variability (soil quality and
18 slope/drainage) within the same vegetation type (Ise an Sato, 2008).

19 To conclude, this work is a step forward in terms of multiple data streams assimilation that
20 opens new perspectives for a better understanding of the carbon cycle and better predictions
21 of the fate of the land carbon sink in the 21st century as a consequence of anthropogenic
22 changes. As ORCHIDEE is part of the IPSL earth system model the impact of the
23 optimization on future climate change predictions will be assessed in a future study. However,
24 we first need to run the ORCHIDAS with a longer atmospheric CO₂ record (i.e. several
25 decades) in order to provide stronger constraints on parameters controlling the impact of
26 climate extremes on the net carbon fluxes at continental to global scales, and the sensitivity of
27 photosynthesis to increasing CO₂ concentration. The optimized model will allow a more in-
28 depth investigation of the trend and inter-annual variations of land surface C fluxes at
29 continental to regional scales, as well as their driving mechanisms. It will offer a more
30 reliable and robust process-based diagnostic of the land C cycle that is compatible with
31 current major data streams. Overall, we have illustrated the benefit of combining multiple
32 data streams in a process-based model to optimize different processes of the model, related to
33 different temporal and spatial scales. The optimization will be updated regularly as new

1 processes are integrated into the ORCHIDEE model, such as for instance land management
2 (Naudts et al., 2015).

3

4 **Code availability**

5 The ORCHIDEE model code and the run environment are open source
6 (<http://forge.ipsl.jussieu.fr/orchidee>) and the associated documentation can be found at
7 <https://forge.ipsl.jussieu.fr/orchidee/wiki/Documentation>. Note that the tangent linear version
8 of the ORCHIDEE model has been generated using commercial software (TAF;
9 <http://www.fastopt.com/products/taf/taf.shtml>). For this reason, only the “forward” version of
10 the ORCHIDEE model is available for sharing. The optimization scheme (in Python) is
11 available through a dedicated web site for data assimilation with ORCHIDEE
12 (<http://orchidas.lsce.ipsl.fr/>). Nevertheless readers interested in running ORCHIDEE are
13 encouraged to contact the corresponding author for full details and latest bug fixes. Finally,
14 the source code of the LMDZ atmospheric transport model can be found at
15 <http://web.lmd.jussieu.fr/trac>.

16

17 **Appendix**

18 **A1. Ocean fluxes**

19 Figure A1 displays the air-sea fluxes from the statistical model.

20 **A2. Fire fluxes**

21 In order to account for fundamental differences between six fire flux categories provided by
22 the GFED product, we grouped these emissions into 3 types with specific treatments. The first
23 group includes C emissions from deforestation and peat fires, which are considered to be
24 permanent carbon lost to the atmosphere, at least over the considered time scales. These
25 fluxes are rescaled to an annual emission of 1.1 PgC.yr^{-1} globally following typical values
26 reported in the literature for deforestation (Houghton R., 2003). The second group consists of
27 C emissions from agriculture and savannah fires, which are compensated by a C sink during
28 the regrowth of these biomes (i.e., savannah and some type of plants on the farmland). These
29 effects are not completely accounted for in ORCHIDEE as the model does not simulate

1 savannah and agriculture fire. Hence, the emissions over the whole period and for each pixel
2 become zero, but their seasonal variations are used. The final group includes emissions from
3 woodland and burnt forests. We considered that at steady state and for a given region certain
4 forests burn but that nearby forests are re-growing following older fires. We thus imposed
5 regrowth at the region scale given that the ORCHIDEE model version that we use does not
6 account for such regrowth. The main assumption is that over century time scale the
7 forest/woodland system is at steady state over a given region (few thousand square km), i.e.
8 there is no net deforestation. We selected an ensemble of small regions over which we
9 calculated the regrowth of these biomes. The derived emissions over the whole period and for
10 each region thus become zero; though we include their spatial and temporal variations. The
11 overall biomass burning flux considered in the CCDAS for the optimization process is the
12 sum of the three fluxes as described above.

13 **A3. Multipliers of the soil initial carbon pools**

14 Figure A2 provides the optimized values of the $K_{soilC,reg}$ parameters that optimize the initial
15 soil carbon pool sizes.

16 .

17 **Acknowledgements**

18 This work was mainly funded by the EU FP7 CARBONES project (contracts FP7-SPACE-
19 2009-1-242316), with also a small contribution from GEOCARBON project
20 (ENV.2011.4.1.1-1-283080). This work used eddy covariance data acquired by the
21 FLUXNET community and in particular by the following networks: AmeriFlux (U.S.
22 Department of Energy, Biological and Environmental Research, Terrestrial Carbon Program
23 (DE-FG02-04ER63917 and DE-FG02-04ER63911)), AfriFlux, AsiaFlux, CarboAfrica,
24 CarboEuropeIP, CarboItaly, CarboMont, ChinaFlux, Fluxnet-Canada (supported by CFCAS,
25 NSERC, BIOCAP, Environment Canada, and NRCan), GreenGrass, KoFlux, LBA, NECC,
26 OzFlux, TCOS-Siberia, USCCC. We acknowledge the financial support to the eddy
27 covariance data harmonization provided by CarboEuropeIP, FAO-GTOS-TCO, iLEAPS, Max
28 Planck Institute for Biogeochemistry, National Science Foundation, University of Tuscia,
29 Université Laval and Environment Canada and US Department of Energy and the database
30 development and technical support from Berkeley Water Center, Lawrence Berkeley National
31 Laboratory, Microsoft Research eScience, Oak Ridge National Laboratory, University of
32 California-Berkeley, University of Virginia. P. C. acknowledges support from the European

1 Research Council through Synergy grant ERC-2013-SyG-610028 “IMBALANCE-P ». The
2 MODIS MOD09CMG collection 5 surface reflectance data are freely available to download
3 from the Land Processes Distributed Active Archive Center (LP DAAC) data portal
4 (<https://lpdaac.usgs.gov>). The authors wish to thank M. Jung for providing access to the GPP
5 MTE data, which were downloaded from the GEOCARBON data portal ([https://www.bgc-](https://www.bgc-jena.mpg.de/geodb/projects/Data.php)
6 [jena.mpg.de/geodb/projects/Data.php](https://www.bgc-jena.mpg.de/geodb/projects/Data.php)). The authors are also grateful to computing support and
7 resources provided at LSCE and to the overall ORCHIDEE project that coordinate the
8 development of the code (<http://labex.ipsl.fr/orchidee/index.php/about-the-team>).

9

10

11

12

13

14

15

16

1 References

- 2 Alton, P. B.: From site-level to global simulation: Reconciling carbon, water and energy
3 fluxes over different spatial scales using a process-based ecophysiological land-surface
4 model, *Agric. For. Meteorol.*, 176, 111–124, doi:10.1016/j.agrformet.2013.03.010, 2013.
- 5 Avitabile V, Herold M, Heuvelink G, Lewis SL, Phillips OL, Asner GP et al. (2015). An
6 integrated pan-tropical biomass maps using multiple reference datasets. *Global Change*
7 *Biology*.
- 8 Bacour, C., Peylin, P., MacBean, N., Rayner, P. J., Delage, F., Chevallier, F., Weiss, M.,
9 Demarty, J., Santaren, D., Baret, F., Berveiller, D., Dufrêne, E. and Prunet, P.: Joint
10 assimilation of eddy covariance flux measurements and FAPAR products over temperate
11 forests within a process-oriented biosphere model, *J. Geophys. Res. Biogeosciences*, 120, 1–
12 19, doi:10.1002/2015JG002966, 2015.
- 13 [Bloom, A. A., Exbrayat, J.-F., van der Velde, I. R., Feng, L. and Williams, M.: The decadal
14 state of the terrestrial carbon cycle: Global retrievals of terrestrial carbon allocation, pools,
15 and residence times., *Proc. Natl. Acad. Sci. U. S. A.*, 113\(5\), 1285– 1290,
16 doi:10.1073/pnas.1515160113, 2016.](#)
- 17 Bousquet P., D. Hauglustaine, P. Peylin, C. Carouge, and P. Ciais, Two decades of OH
18 variability as inferred by an inversion of atmospheric transport and chemistry of methyl
19 chloroform, *Atmos. Chem. and Phys.*, 5, 263-2656, ISI:000232370800002, 2005.
- 20 Braswell, B. H., Sacks, W. J., Linder, E. and Schimel, D. S.: Estimating diurnal to annual
21 ecosystem parameters by synthesis of a carbon flux model with eddy covariance net
22 ecosystem exchange observations, *Glob. Change Biol.*, 11(2), 335–355, doi:10.1111/j.1365-
23 2486.2005.00897.x, 2005.
- 24 Byrd, R. H., P. Lu, J. Nocedal, and C. Zhu (1995), A limited memory algorithm for bound
25 constrained optimization, *SIAM J. Sci. Stat. Comput.*, 16(5), 1190–1208.
- 26 Canadell, J. G., Ciais, P., Sabine, C., and Joos, F. (Eds.): REgional Carbon Cycle Assessment
27 and Processes (RECCAP), Special issue, *Biogeosciences*, [http://www.biogeosciences-](http://www.biogeosciences-discuss.net/special_issue83.html)
28 [discuss.net/ special_issue83.html](http://www.biogeosciences-discuss.net/special_issue83.html), 2013.
- 29 Chevallier F., Fisher M., Peylin P., Serrar S., Bousquet P., Bréon F-M., Chédin A., Ciais P.
30 (2005), Inferring CO₂ sources and sinks from satellite observations: Method and application
31 to TOVS data, *Journal of Geophysical Research*, **110**, D24309, doi:20.1029/2005JD006390,
32 13pp.
- 33 Chevallier, F., P. Ciais, T. J. Conway, T. Aalto, B. E. Anderson, P. Bousquet, E. G. Brunke,
34 L. Ciattaglia, Y. Esaki, M. Fröhlich, A.J. Gomez, A.J. Gomez-Pelaez, L. Haszpra, P.
35 Krummel, R. Langenfelds, M. Leuenberger, T. Machida, F. Maignan, H. Matsueda, J. A.
36 Morguí, H. Mukai, T. Nakazawa, P. Peylin, M. Ramonet, L. Rivier, Y. Sawa, M. Schmidt, P.
37 Steele, S. A. Vay, A. T. Vermeulen, S. Wofsy, D. Worthy, (2010), CO₂ surface fluxes at grid
38 point scale estimated from a global 21-year reanalysis of atmospheric measurements, *Journal*
39 *of Geophysical Research*, **115**, D21307, doi:10.1029/2010JD013887.

- 1 Collatz GJ, Ribas-Carbo M, Berry JA, (1992), Coupled Photosynthesis-Stomatal Conductance
2 Model for Leaves of C4 Plants. *Aust J Plant Physiol*, **19**: 519-38.
- 3 de Rosnay P, Polcher J. (1998), Modelling root water uptake in a complex land surface
4 scheme coupled to a GCM. *Hydrol Earth Syst Sc*, **2**: 239-55.
- 5 Dee, D. P., Uppala, S. M., Simmons, A. J., Berrisford, P., Poli, P., Kobayashi, S., Andrae, U.,
6 Balmaseda, M. A., Balsamo, G., Bauer, P., Bechtold, P., Beljaars, A. C. M., van de Berg, L.,
7 Bidlot, J., Bormann, N., Delsol, C., Dragani, R., Fuentes, M., Geer, A. J., Haimberger, L.,
8 Healy, S. B., Hersbach, H., Hólm, E. V., Isaksen, I., Kållberg, P., Köhler, M., Matricardi, M.,
9 McNally, A. P., Monge-Sanz, B. M., Morcrette, J. J., Park, B. K., Peubey, C., de Rosnay, P.,
10 Tavolato, C., Thépaut, J. N., and Vitart, F.: The ERA-interim reanalysis: configuration and
11 performance of the data assimilation system, *Q. J. Roy. Meteor. Soc.*, **137**, 553–597,
12 doi:10.1002/qj.828, 2011.
- 13 Ducoudre NI, Laval K, Perrier A. Sechiba (1993), A New Set of Parameterizations of the
14 Hydrologic Exchanges at the Land Atmosphere Interface within the Lmd Atmospheric
15 General-Circulation Model. *J Climate*, **6**: 248-73.
- 16 Dufresne, J.-L., et al. (2011), Climate change projections using the IPSL-CM5 Earth System
17 Model: from CMIP3 to CMIP5, submitted to *Clim. Dynam.*
- 18 Farquhar, G. D., von Caemmerer, S. von and Berry, J. A.: A biochemical model of
19 photosynthetic CO₂ assimilation in leaves of C3 species, *Planta*, **149**(1), 78–90, 1980.
- 20 Folberth G., Hauglustaine D.A., Ciais P., et al. (2005), On the role of atmospheric chemistry
21 in the global CO₂ budget, *Geophysical Research Letters*, **32**(8): L08801
- 22 Fung, I. Y., C. J. Tucker, and K. C. Prentice, Application of Advanced Very High Resolution
23 Radiometer vegetation index to study atmosphere – biosphere exchange of CO₂, *J. Geophys.*
24 *Res.*, **92**, 2999– 3015, 1987.
- 25 GLOBALVIEW : Cooperative Global Atmospheric Data Integration Project. 2013, updated
26 annually. Multi-laboratory compilation of synchronized and gap-filled atmospheric carbon
27 dioxide records for the period 1979-2012 (obspack_co2_1_GLOBALVIEW-
28 CO2_2013_v1.0.4_2013-12-23). Compiled by NOAA Global Monitoring Division: Boulder,
29 Colorado, U.S.A. Data product accessed at <http://dx.doi.org/10.3334/OBSPACK/1002>.
- 30 Groenendijk, M., Dolman, a. J., van der Molen, M. K., Leuning, R., Arneeth, a., Delpierre,
31 N., Gash, J. H. C., Lindroth, a., Richardson, a. D., Verbeeck, H. and Wohlfahrt, G.:
32 Assessing parameter variability in a photosynthesis model within and between plant
33 functional types using global Fluxnet eddy covariance data, *Agric. For. Meteorol.*, **151**(1),
34 22–38, doi:10.1016/j.agrformet.2010.08.013, 2011.
- 35 Hauglustaine D.A., Hourdin F., Jourdain L., et al. (2004), Interactive chemistry in the
36 Laboratoire de Meteorologie Dynamique general circulation model: Description and
37 background tropospheric chemistry evaluation, *Journal of Geophysical Research -*
38 *Atmosphere*, **109**(D4): D04314

1 Houghton, R. A. (2003) Revised estimates of the annual net flux of carbon to the atmosphere
2 from changes in land use and land management 1850-2000. *Tellus* **55B**: 378-390.

3 Hourdin F. and Armengaud A. (1999), The use of finite-volume methods for atmospheric
4 advection of trace species. Part I: Test of various formulations in a general circulation
5 model, *Monthly Weather Review*, **127**(5): 822-837

6 Hourdin, F. et al. (2006), The LMDZ4 general circulation model: climate performance and
7 sensitivity to parametrized physics with emphasis on tropical convection, *Climate*
8 *Dynamics*, **27**(7), 787-813, 2006.

9 IPCC, (2007). Climate Change 2007: The Physical Science Basis. Contribution of Working
10 Group I to the Fourth Assessment Report of the Intergovernmental Panel on Climate Change
11 [Solomon, S., D. Qin, M. Manning (eds.)]

12 [Ise, T., and H. Sato, Representing subgrid-scale edaphic heterogeneity in a largescale
13 ecosystem model: A case study in the circumpolar boreal regions, *Geophys. Res. Lett.*, **35**,
14 L20407, doi:10.1029/2008GL035701, 2008.](#)

15 Kaminski, T., Knorr, W., Scholze, M., Gobron, N., Pinty, B., Giering, R. and Mathieu, P-P.
16 (2012), Consistent assimilation of MERIS FAPAR and atmospheric CO₂ into a terrestrial
17 vegetation model and interactive mission benefit analysis, *Biogeosciences*, **9**, 3173-3184.

18 Kaminski, T., Knorr, W., Schürmann, G., Scholze, M., Rayner, P. J., Zaehle, S., Blessing, S.,
19 Dorigo, W., Gayler, V., Giering, R., Gobron, N., Grant, J. P., Heimann, M., Hooker-Stroud,
20 a., Houweling, S., Kato, T., Kattge, J., Kelley, D., Kemp, S., Koffi, E. N., Köstler, C.,
21 Mathieu, P. P., Pinty, B., Reick, C. H., Rödenbeck, C., Schnur, R., Scipal, K., Sebald, C.,
22 Stacke, T., Van Scheltinga, a. T., Vossbeck, M., Widmann, H. and Ziehn, T.: The
23 BETHY/JSBACH Carbon Cycle Data Assimilation System: Experiences and challenges, *J.*
24 *Geophys. Res. Biogeosciences*, **118**(4), 1414–1426, doi:10.1002/jgrg.20118, 2013.

25 Kato, T., Knorr, W., Scholze, M., Veenendaal, E., Kaminski, T., Kattge, J. and Gobron, N.:
26 Simultaneous assimilation of satellite and eddy covariance data for improving terrestrial water
27 and carbon simulations at a semi-arid woodland site in Botswana, *Biogeosciences*, **10**(2),
28 789–802, doi:10.5194/bg-10-789-2013, 2013.

29 Keenan, T. F., Davidson, E. a., Munger, J. W. and Richardson, A. D.: Rate my data:
30 Quantifying the value of ecological data for the development of models of the terrestrial
31 carbon cycle, *Ecol. Appl.*, **23**(1), 273–286, doi:10.1890/12-0747.1, 2013.

32 Keenan, T. F., Davidson, E., Moffat, A. M., Munger, W. and Richardson, A. D.: Using
33 model-data fusion to interpret past trends, and quantify uncertainties in future projections, of
34 terrestrial ecosystem carbon cycling, *Glob. Change Biol.*, **18**(8), 2555–2569,
35 doi:10.1111/j.1365-2486.2012.02684.x, 2012.

36 Knorr, W. and Kattge, J.: Inversion of terrestrial ecosystem model parameter values against
37 eddy covariance measurements by Monte Carlo sampling, *Glob. Change Biol.*, **11**(8), 1333–
38 1351, doi:10.1111/j.1365-2486.2005.00977.x, 2005.

Philippe Peylin 4/6/16 16:58
Mis en forme: Police :12 pt

Philippe Peylin 4/6/16 16:58
Mis en forme: Police :12 pt

Philippe Peylin 4/6/16 16:58
Mis en forme: Motif : Transparente

- 1 Knyazikhin, Y., Martonchik, J.V., Myneni, R.B., Diner, D.J., and Running, S.W. (1998),
2 Synergistic algorithm for estimating vegetation canopy leaf area index and fraction of
3 absorbed photosynthetically active radiation from MODIS and MISR, *Journal of Geophysical*
4 *Research*, **103**, D24, 32,257-32,276.
- 5 Koffi, E. N., Rayner, P. J., Scholze, M., & Beer, C. (2012). Atmospheric constraints on gross
6 primary productivity and net ecosystem productivity: Results from a carbon cycle data
7 assimilation system. *Global biogeochemical cycles*, 26(1).
- 8 Krinner, G., Viovy, N., de Noblet-Ducoudré, N., Ogée, J., Polcher, J., Friedlingstein, P.,
9 Ciais, P., Sitch, S. and Prentice, I. C.: A dynamic global vegetation model for studies of the
10 coupled atmosphere-biosphere system, *Glob. Biogeochem. Cycles*, 19(1) [online] Available
11 from: <http://onlinelibrary.wiley.com/doi/10.1029/2003GB002199/pdf> (Accessed 23
12 November 2015), 2005.
- 13 Kuppel, S., Chevallier, F. and Peylin, P.: Quantifying the model structural error in carbon
14 cycle data assimilation systems, *Geosci. Model Dev.*, 6(1), 45–55, doi:10.5194/gmd-6-45-
15 2013, 2013.
- 16 Kuppel, S., Peylin, P., Chevallier, F., Bacour, C., Maignan, F. and Richardson, A. D.:
17 Constraining a global ecosystem model with multi-site eddy-covariance data, *Biogeosciences*,
18 9(10), 3757–3776, doi:10.5194/bg-9-3757-2012, 2012.
- 19 Kuppel, S., Peylin, P., Maignan, F., Chevallier, F., Kiely, G., Montagnani, L. and Cescatti, A.:
20 Model–data fusion across ecosystems: from multisite optimizations to global simulations,
21 *Geosci. Model Dev.*, 7(6), 2581–2597, 2014.
- 22 Lasslop, G., M. Reichstein, D. Papale, A. D. Richardson, A. Arneth, A. Barr, P. Stoy, and G.
23 Wohlfahrt. 2010. Separation of net ecosystem exchange into assimilation and respiration
24 using a light response curve approach: critical issues and global evaluation. *Global Change*
25 *Biology*, **16**, 187-208.
- 26 Lasslop, G., M. Reichstein, J. Kattge, and D. Papale. 2008. Influences of observation errors in
27 eddy flux data on inverse model parameter estimation. *Biogeosciences*, **5**, 1311-1324.
- 28 Le Quéré, C., Moriarty, R., Andrew, R. M., Peters, G. P., Ciais, P., Friedlingstein, P., Jones,
29 S. D., Sitch, S., Tans, P., Arneth, a., Boden, T. a., Bopp, L., Bozec, Y., Canadell, J. G., Chini,
30 L. P., Chevallier, F., Cosca, C. E., Harris, I., Hoppema, M., Houghton, R. a., House, J. I., Jain,
31 a. K., Johannessen, T., Kato, E., Keeling, R. F., Kitidis, V., Klein Goldewijk, K., Koven, C.,
32 Landa, C. S., Landschützer, P., Lenton, a., Lima, I. D., Marland, G., Mathis, J. T., Metzl, N.,
33 Nojiri, Y., Olsen, a., Ono, T., Peng, S., Peters, W., Pfeil, B., Poulter, B., Raupach, M. R.,
34 Regnier, P., Rödenbeck, C., Saito, S., Salisbury, J. E., Schuster, U., Schwinger, J., Séférian,
35 R., Segschneider, J., Steinhoff, T., Stocker, B. D., Sutton, a. J., Takahashi, T., Tilbrook, B.,
36 van der Werf, G. R., Viovy, N., Wang, Y.-P., Wanninkhof, R., Wiltshire, a. and Zeng, N.:
37 Global carbon budget 2014, *Earth Syst. Sci. Data*, 7(1), 47–85, doi:10.5194/essd-7-47-2015,
38 2015.

- 1 Liss, P. and Merlivat, L. (1986). The role of sea-air exchange in geochemical cycling, Ed. P.
2 Menard, chapter Air-sea gas exchange rates: Introduction and synthesis, pages 113-127.
3 Reidel, Dordrecht.
- 4 MacBean, N., Maignan, F., Peylin, P., Bacour, C., François-Marie, B. and Ciais, P.: Using
5 satellite data to improve the leaf phenology of a global Terrestrial Biosphere Model,
6 *Biogeosciences*, 12, 7185-7208, 2015.
- 7 MacBean, N., Peylin, P., Chevallier, F., Scholze, M. and G. Schürmann, Consistent
8 assimilation of multiple data streams in a Carbon Cycle Data Assimilation System,
9 *Biogeosciences*, submitted, 2016.
- 10 Madec, G., P. Delecluse, M. Imbard and C. Lévy, 1998 : OPA 8.1 Ocean General Circulation
11 Model reference manual, Note du Pole de Modelisation, Institut Pierre-Simon Laplace, 11,
12 91pp.
- 13 Maignan, F., Bréon, F.-M., Chevallier, F., Viovy, N., Ciais, P., Garrec, C., Trules, J., and
14 Mancip, M.: Evaluation of a Global Vegetation Model using time series of satellite vegetation
15 indices, *Geosci. Model Dev.*, 4, 1103-1114, doi:10.5194/gmd-4-1103-2011, 2011.
- 16 Moore, D. J. P., Hu, J., Sacks, W. J., Schimel, D. S. and Monson, R. K.: Estimating
17 transpiration and the sensitivity of carbon uptake to water availability in a subalpine forest
18 using a simple ecosystem process model informed by measured net CO₂ and H₂O fluxes,
19 *Agric. For. Meteorol.*, 148(10), 1467–1477, doi:10.1016/j.agrformet.2008.04.013, 2008.
- 20 Naudts, K., Ryder, J., J McGrath, M., Otto, J., Chen, Y., Valade, A., ... & Ghattas, J. (2015).
21 A vertically discretised canopy description for ORCHIDEE (SVN r2290) and the
22 modifications to the energy, water and carbon fluxes. *Geoscientific Model Development*, 8,
23 2035-2065.
- 24 Nightingale, P.D., et al. 2000. In situ evaluation of air-sea gas exchange parameterizations
25 using novel conservative and volatile tracers. *Glob. Biogeochem Cycles*, **14**, 373-387.
- 26 Olson, J., Watts, J.A., and Allison, L.J. (1983), Carbon in Live Vegetation of Major World
27 Ecosystems, ORNL-5862, Oak Ridge National Laboratory, Oak Ridge, Tennessee, 164pp.
- 28 Papale, D. (2006), Towards a standardized processing of Net Ecosystem Exchange measured
29 with eddy covariance technique: algorithms and uncertainty estimation, [online] Available
30 from: <http://dSPACE.unitus.it/handle/2067/1321> (Accessed 27 August 2013)
- 31 Parton W, Stewart J, Cole C, (1988), Dynamics of C, N, P and S in grassland soils: a model.
32 *Biogeochemistry*, **5**: 109-31.
- 33 Peylin P, Rayner PJ, Bousquet P, et al. (2005), Daily CO₂ flux estimates over Europe from
34 continuous atmospheric measurements: 1, inverse methodology, *Atmospheric Chemistry and
35 Physics*, **5**: 3173-3186.
- 36 Piao, S., Sitch, S., Ciais, P., Friedlingstein, P., Peylin, P., Wang, X., Ahlström, A., Anav, A.,
37 Canadell, J. G., Cong, N., Huntingford, C., Jung, M., Levis, S., Levy, P. E., Li, J., Lin, X.,

- 1 Lomas, M. R., Lu, M., Luo, Y., Ma, Y., Myneni, R. B., Poulter, B., Sun, Z., Wang, T., Viovy,
2 N., Zaehle, S. and Zeng, N.: Evaluation of terrestrial carbon cycle models for their response to
3 climate variability and to CO₂ trends, *Glob. Change Biol.*, 19(7), 2117–2132,
4 doi:10.1111/gcb.12187, 2013.
- 5 Prentice, I. C., Liang, X., Medlyn, B. E. and Wang, Y.-P.: Reliable, robust and realistic: the
6 three R's of next-generation land-surface modelling, *Atmospheric Chem. Phys.*, 15(10),
7 5987–6005, doi:10.5194/acp-15-5987-2015, 2015.
- 8 Rayner, P. J., Scholze, M., Knorr, W., Kaminski, T., Giering, R. and Widmann, H.: Two
9 decades of terrestrial carbon fluxes from a carbon cycle data assimilation system (CCDAS), ,
10 19, doi:10.1029/2004GB002254, 2005.
- 11 Rayner, P. J. (2010). The current state of carbon-cycle data assimilation. *Current Opinion in*
12 *Environmental Sustainability*, 2(4), 289-296.
- 13 Regnier, P., Friedlingstein, P., Ciais, P., Mackenzie, F. T., Gruber, N., Janssens, I. A., ... &
14 Arndt, S. (2013). Anthropogenic perturbation of the carbon fluxes from land to ocean. *Nature*
15 *Geoscience*, 6(8), 597-607.
- 16 Ricciuto, D. M., A. W. King, D. Dragoni, and W. M. Post (2011), Parameter and prediction
17 uncertainty in an optimized terrestrial carbon cycle model: Effects of constraining variables
18 and data record length, *J. Geophys. Res.*, 116, G01033, doi:10.1029/2010JG001400.
- 19 Ricciuto, D. M., Butler, M. P., Davis, K. J., Cook, B. D., Bakwin, P. S., Andrews, A. and
20 Teclaw, R. M.: Causes of interannual variability in ecosystem-atmosphere CO₂ exchange in a
21 northern Wisconsin forest using a Bayesian model calibration, *Agric. For. Meteorol.*, 148(2),
22 309–327, doi:10.1016/j.agrformet.2007.08.007, 2008.
- 23 Richardson, A. D., Williams, M., Hollinger, D. Y., Moore, D. J. P., Dail, D. B., Davidson, E.
24 a., Scott, N. a., Evans, R. S., Hughes, H., Lee, J. T., Rodrigues, C. and Savage, K.: Estimating
25 parameters of a forest ecosystem C model with measurements of stocks and fluxes as joint
26 constraints, *Oecologia*, 164(1), 25–40, doi:10.1007/s00442-010-1628-y, 2010.
- 27 Rivier L., Ciais P., Hauglustaine D.A., et al. (2006), Evaluation of SF₆, C₂Cl₄, and CO to
28 approximate fossil fuel CO₂ in the Northern Hemisphere using a chemistry transport
29 model, *Journal Geophysical Research-Atmosphere*, **111**(D16) - D16311.
- 30 Rödenbeck, C., T. J. Conway, and R. L. Langenfelds (2006), The effect of systematic
31 measurement errors on atmospheric CO₂ inversions: A quantitative assessment, *Atmos.*
32 *Chem. Phys.*, **6**, 149–161, doi:10.5194/acp-6-149-2006.
- 33 Rödenbeck C., D.C.E. Bakker, N. Gruber, Y. Iida, A. Jacobson, S. Jones, P. Landschutzer, N.
34 Metzl, S. Nakaoka, A. Olsen, G.-H. Park, P. Peylin, K.B. Rodgers, T.P. Sasse, U. Schuster,
35 J.D. Shutler, V. Valsala, R. Wanninkhof, and J. Zeng, 2015. Data-based estimates of the
36 ocean carbon sink variability – First results of the Surface Ocean pCO₂ Mapping
37 intercomparison (SOCOM). *Biogeosciences*, 12: 7251-7278. doi:10.5194/bg-12-7251-2015.

- 1 Rosenblatt, F. (1958). The perceptron: a probabilistic model for information storage and
2 organization in the brain. *Psychological review*, 65(6), 386.
- 3 Ruimy A, Dedieu G, Saugier B, (1996), TURC: A diagnostic model of continental gross
4 primary productivity and net primary productivity. *Global Biogeochemical Cycles*, 10: 269-
5 85.
- 6 Sabine, C.L., et al. 2004. The oceanic sink for anthropogenic CO₂. *Science*, 305 (5682), 367-
7 371.
- 8 [Saito, M., A. Ito and S. Maksyutov, Optimization of a prognostic biosphere model for terrestrial
9 biomass and atmospheric CO2 variability, *Geosci. Model Dev.*, 7, 1829-1840, doi:10.5194/gmd-7-
10 1829-2014, 2014.](#)
- 11 Santaren, D., Peylin, P., Bacour, C., Ciais, P. and Longdoz, B.: Ecosystem model
12 optimization using in situ flux observations: benefit of Monte Carlo versus variational
13 schemes and analyses of the year-to-year model performances, *Biogeosciences*, 11(24), 7137-
14 7158, 2014.
- 15 Sitch, S., Friedlingstein, P., Gruber, N., Jones, S. D., Murray-Tortarolo, G., Ahlström, A.,
16 Doney, S. C., Graven, H., Heinze, C., Huntingford, C., Levis, S., Levy, P. E., Lomas, M.,
17 Poulter, B., Viovy, N., Zaehle, S., Zeng, N., Arneeth, A., Bonan, G., Bopp, L., Canadell, J. G.,
18 Chevallier, F., Ciais, P., Ellis, R., Gloor, M., Peylin, P., Piao, S., Le Quéré, C., Smith, B.,
19 Zhu, Z. and Myneni, R.: Recent trends and drivers of regional sources and sinks of carbon
20 dioxide, *Biogeosciences*, 12, 653–679, doi:10.5194/bgd-12-653-2015, 2015.
- 21 Takahashi, et al. 2009, Corrigendum to "Climatological mean and decadal change in surface
22 ocean pCO₂, and net sea-air CO₂ flux over the global oceans" *Deep Sea Res. II*, 56, 554-577.
- 23 Tarantola A. (1987), *Inverse problem theory: Methods for data fitting and parameter
24 estimation*. Elsevier, Amsterdam.
- 25 Tarantola, A. (2005), *Inverse problem theory and methods for model parameters
26 estimation, Society for Industrial and Applied Mathematics*, Philadelphia, ISBN 0-89871-572-
27 5.
- 28 Thum, T., MacBean, N., Peylin, P., Bacour, C., Santaren, D., Longdoz, B., Loustau, D. and
29 Ciais, P., The potential of forest biomass data in addition to carbon and water flux
30 measurements to constrain ecosystem model parameters: Case studies at two temperate forest
31 sites, *Agriculture and Forest Meteorology*, in revision, 2015.
- 32 Tiedtke M. (1989), A comprehensive mass flux scheme for cumulus parameterization in
33 large-scale models, *Monthly Weather Review*, 117(8): 1779-1800
- 34 Tucker, C. J. (1979). Red and photographic infrared linear combinations for monitoring
35 vegetation. *Remote Sensing of Environment*, 8, 127-150.
- 36 Twine, T. E., W. P. Kustas, J. M. Norman, D. R. Cook, P. R. Houser, T. P. Meyers, J. H.
37 Prueger, P. J. Starks, and M. L. Wesely (2000), Correcting eddy-covariance flux

1 underestimates over a grassland, *Agric. For. Meteorol.*, 103(3), 279–300, doi:10.1016/S0168-
2 1923(00)00123-4.

3 Verant, S., Laval, K., Polcher, J., and De Castro, M. (2004), Sensitivity of the continental
4 hydrological cycle to the spatial resolution over the Iberian Peninsula, *Journal of*
5 *Hydrometeorology*, 5, 267-285.

6 Vermote, E., C.O. Justice and F-M Breon (2009), Towards a generalized approach for
7 correction of the BRDF effect in MODIS directional reflectances, *IEEE Transactions on*
8 *Geoscience and Remote Sensing*, 47, 3, 898-908.

9 Wang, Y. P., Baldocchi, D., Leuning, R., Falge, E. and Vesala, T.: Estimating parameters in a
10 land-surface model by applying nonlinear inversion to eddy covariance flux measurements
11 from eight FLUXNET sites, *Glob. Change Biol.*, 13(3), 652–670, doi:10.1111/j.1365-
12 2486.2006.01225.x, 2007.

13 Wang, Y. P., Leuning, R., Cleugh, H. and Coppin, P.: Parameter estimation in surface
14 exchange models using nonlinear inversion : how many parameters can we estimate and
15 which measurements are most useful ?, *Glob. Change Biol.*, 7, 495–510, doi:10.1046/j.1365-
16 2486.2001.00434.x, 2001.

17 Wanninkhof, R., 1992. Relationship between wind speed and gas exchange. *J. Geophys.*
18 *Res.* 97, 7373-7382.

19 Weiss, R.F., 1974. Carbon dioxide in water and seawater: the solubility of a non-ideal gas.
20 *Mar. Chem.*, 2, 203-215.

21 Welp, L. R., Keeling, R. F., Meijer, H. A., Bollenbacher, A. F., Piper, S. C., Yoshimura, K.,
22 ... & Wahlen, M. (2011). Interannual variability in the oxygen isotopes of atmospheric CO₂
23 driven by El Nino. *Nature*, 477(7366), 579-582.

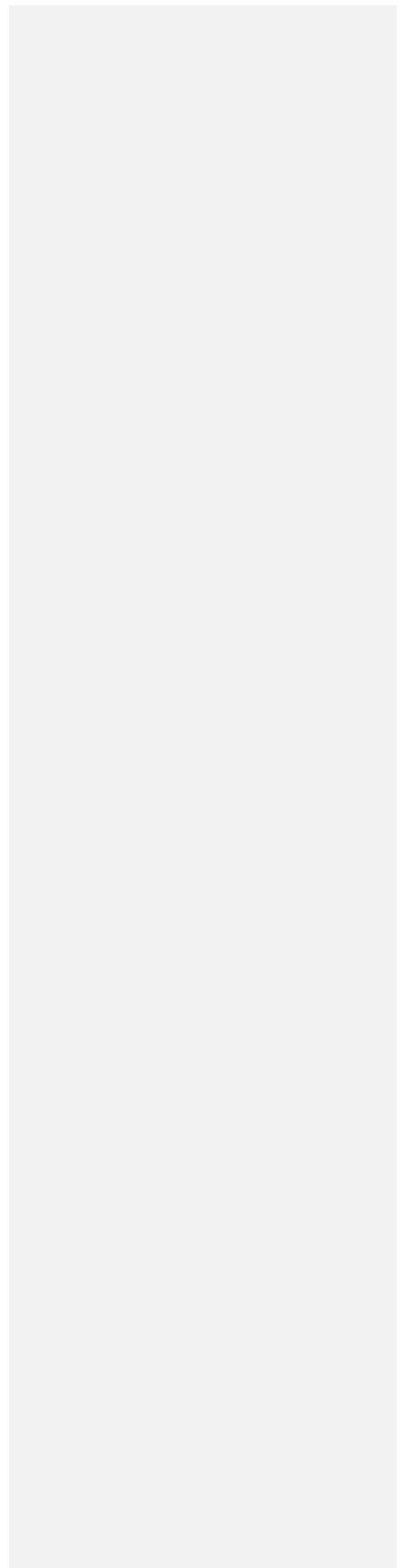
24 Williams, M., Schwarz, P. a, Law, B. E., Irvine, J. and Kurpius, M. R.: An improved analysis
25 of forest carbon dynamics using data assimilation, *Glob. Change Biol.*, 11(1), 89–105,
26 doi:10.1111/j.1365-2486.2004.00891.x, 2005.

27 Xiao, J., Davis, K. J., Urban, N. M. and Keller, K.: Uncertainty in model parameters and
28 regional carbon fluxes: A model-data fusion approach, *Agric. For. Meteorol.*, 189-190, 175–
29 186, doi:10.1016/j.agrformet.2014.01.022, 2014.

30 Zobitz, J. M., D. J. P. Moore, T. Quaife, B. H. Braswell, A. Bergeson, J. A. Anthony, and R.
31 K. Monson (2014), Joint data assimilation of satellite reflectance and net ecosystem exchange
32 data constrains ecosystem carbon fluxes at a high-elevation subalpine forest, *Agric. For.*
33 *Meteorol.*, 195–196, 73–88.

34 Zabler, L (1986), A world soil file for global climate modeling, NASA Technical
35 Memorandum 87802. NASA Goddard Institute for Space Studies, New York, U.S.A.

36



1 **Tables**

2 Table 1. Parameters description, generality (PFT dependent, global, specific to FLUXNET
3 sites or for a set of regions) and data stream(s) that were used to constrain them.

Parameter	Description	Dependent	Constraint
V_{cmax}	Maximum carboxylation rate ($\mu\text{mol}\cdot\text{m}^{-2}\cdot\text{s}^{-1}$)	PFT	Flux, CO ₂
$G_{s,slope}$	Ball-Berry slope	PFT	Flux, CO ₂
$C_{T,opt}$	Optimal photosynthesis temperature (°C)	PFT	Flux, CO ₂
SLA	Specific leaf area ($\text{m}^2\cdot\text{g}^{-1}$)	PFT	Flux, CO ₂
$K_{LAI,happy}$	LAI threshold to stop using carbohydrate reserves	PFT	Sat, Flux, CO ₂
$K_{pheno,crit}$	Multiplicative parameter of the threshold that determines the start of the growing season	PFT	Sat, Flux, CO ₂
$L_{age,crit}$	Average critical age of leaves (days)	PFT	Sat, Flux, CO ₂
$C_{T,sen}$	Temperature threshold for senescence (°C)	PFT	Sat, Flux, CO ₂
$F_{stress,h}$	Parameter reducing the hydric limitation of photosynthesis	PFT	Flux, CO ₂
MR_{offset}	Offset of the temperature dependence of maintenance respiration	Global	Flux, CO ₂
Q_{10}	Temperature dependency of heterotrophic respiration	Global	Flux, CO ₂
HR_{Hc}	Offset of the soil/litter moisture control function	Global	Flux, CO ₂
$K_{soilC,site}$	Multiplicative factor of the initial soil carbon pools	per Site	Flux
$K_{soilC,reg}$		30 regions	CO ₂
K_{albedo}	Multiplicative factor of the vegetation albedo	Global	Flux, CO ₂

Philippe Peylin 10/6/16 19:44
Supprimé: 36

4
5
6

- 1 Table 2. Prior information for all parameters except initial soil C pool multipliers: prior value,
- 2 uncertainty and range of variation for the different plant functional types (Tropical Broadleaf
- 3 Evergreen/Raingreen forests (TrBE / TrBR), Temperate Needle leaf / Broadleaf Evergreen
- 4 forests (TeNE, TeBE), Temperate Broadleaf Deciduous forest (TeBD), Boreal Needle leaf
- 5 Evergreen forests (BoNE), Boreal Broadleaf / Needle leaf Deciduous forests (BoBD / BoND)
- 6 and C3 grassland.

Parameter	Plant functional type								
	TrBE	TrBR	TeNE	TeBE	TeBD	BoNE	BoBD	BoND	NC3
V_{max}	65 ± 24 [35; 95]	65 ± 24 [35; 95]	35 ± 12.8 [19; 51]	45 ± 16 [25; 65]	55 ± 20 [30; 80]	35 ± 12.8 [19; 51]	45 ± 16 [25; 65]	35 ± 12.8 [19; 51]	70 ± 25.6 [38; 102]
$G_{s,slope}$	6.0 ± 2.4 [6; 12]	6.0 ± 2.4 [6; 12]	6.0 ± 2.4 [6; 12]	6.0 ± 2.4 [6; 12]	6.0 ± 2.4 [6; 12]	6.0 ± 2.4 [6; 12]	6.0 ± 2.4 [6; 12]	6.0 ± 2.4 [6; 12]	6.0 ± 2.4 [6; 12]
$c_{T,opt}$	37 ± 6.4 [29; 45]	37 ± 6.4 [29; 45]	25 ± 6.4 [17; 33]	32 ± 6.4 [24; 40]	26 ± 6.4 [18; 34]	25 ± 6.4 [17; 33]	25 ± 6.4 [17; 33]	25 ± 6.4 [17; 33]	27.25 ± 6.4 [19.25; 35.25]
SLA	0.015 ± 0.0092 [0.007; 0.03]	0.026 ± 0.0148 [0.013; 0.05]	0.009 ± 0.0064 [0.004; 0.02]	0.02 ± 0.012 [0.01; 0.04]	0.026 ± 0.0148 [0.013; 0.05]	0.009 ± 0.0064 [0.004; 0.02]	0.026 ± 0.0148 [0.013; 0.05]	0.009 ± 0.0064 [0.004; 0.02]	0.026 ± 0.0148 [0.013; 0.05]
$K_{LAI,happy}$	0.50 ± 0.14 [0.35; 0.70]	0.50 ± 0.14 [0.35; 0.70]	0.50 ± 0.14 [0.35; 0.70]	0.50 ± 0.14 [0.35; 0.70]	0.50 ± 0.14 [0.35; 0.70]	0.50 ± 0.14 [0.35; 0.70]	0.50 ± 0.14 [0.35; 0.70]	0.50 ± 0.14 [0.35; 0.70]	0.50 ± 0.14 [0.35; 0.70]
$K_{pheno,crit}$	—	1.0 ± 0.44 [0.7; 1.8]	—	—	1.0 ± 0.44 [0.7; 1.8]	—	1.0 ± 0.44 [0.7; 1.8]	1.0 ± 0.44 [0.7; 1.8]	1.0 ± 0.44 [0.7; 1.8]
$L_{age,crit}$	730 ± 192 [490; 970]	180 ± 48 [120; 240]	910 ± 240 [610; 1210]	730 ± 192 [490; 970]	180 ± 48 [120; 240]	910 ± 240 [610; 1210]	180 ± 48 [120; 240]	180 ± 48 [120; 240]	120 ± 60 [30; 180]
$C_{T,sen}$	—	—	—	—	12 ± 8 [2; 22]	—	7 ± 8 [-3; 17]	2 ± 8 [-8; 12]	-1.375 ± 8 [-11.375; 9.375]
$F_{stress,h}$	6.0 ± 3.2 [2; 10]	6.0 ± 3.2 [2; 10]	6.0 ± 3.2 [2; 10]	6.0 ± 3.2 [2; 10]	6.0 ± 3.2 [2; 10]	6.0 ± 3.2 [2; 10]	6.0 ± 3.2 [2; 10]	6.0 ± 3.2 [2; 10]	6.0 ± 3.2 [2; 10]
MR_{offset}	1.0 ± 0.6 [0.5; 2.0]								
$Q10$	1.99372 ± 0.8 [1.0; 3.0]								
HR_{Hc}	-0.29 ± 0.24 [-0.59; 0.01]								
K_{albedo}	1.0 ± 0.16 [0.8; 1.2]								

1
2
3
4

5
6
7
8

Main Figures

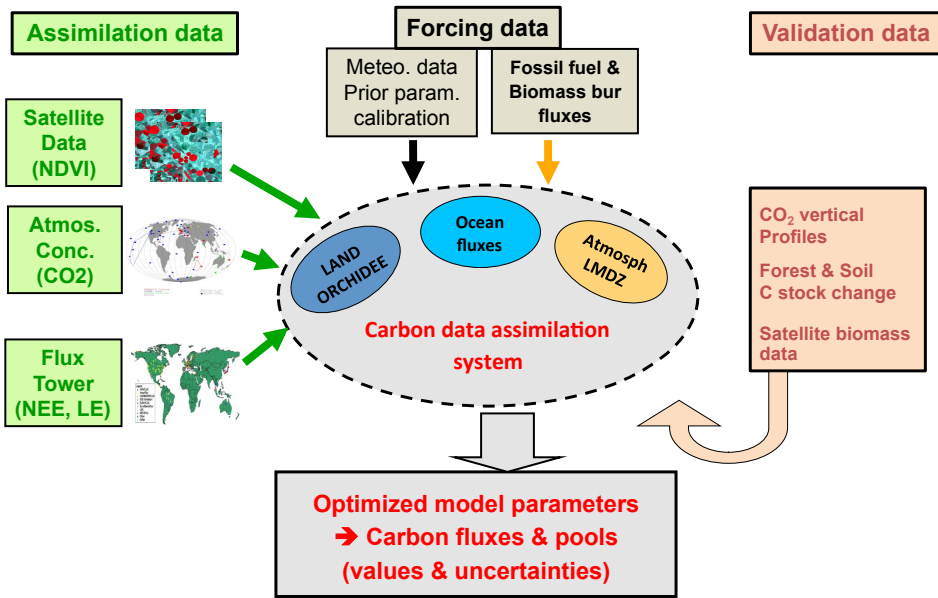
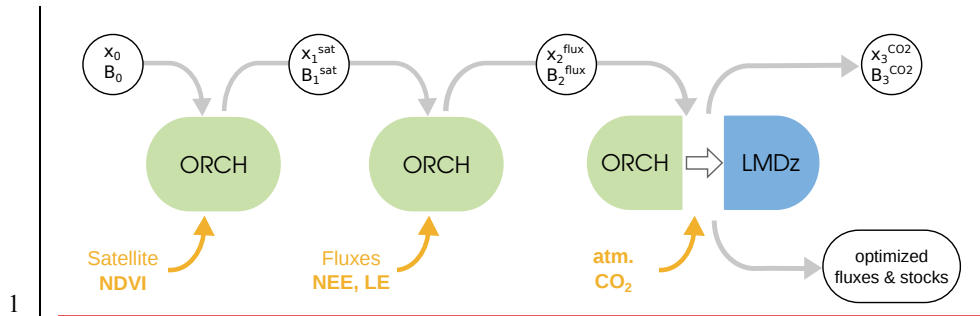


Figure 1. Schematic of the ORCHIDEE Carbon Cycle Data Assimilation System (ORCHIDAS).



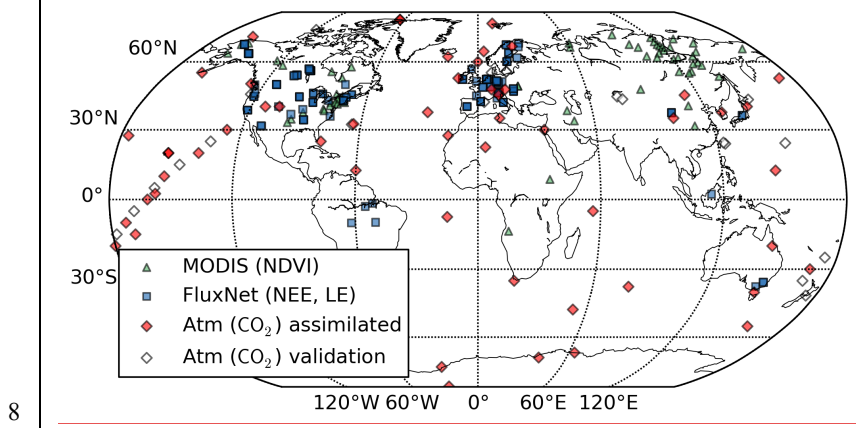
1

2 Figure 2. Illustration of the step-wise data assimilation approach used for the assimilation of
 3 multiple data streams in the ORCHIDEE-CCDAS. The list of parameters for each step is
 4 summarized in Table 1.

5

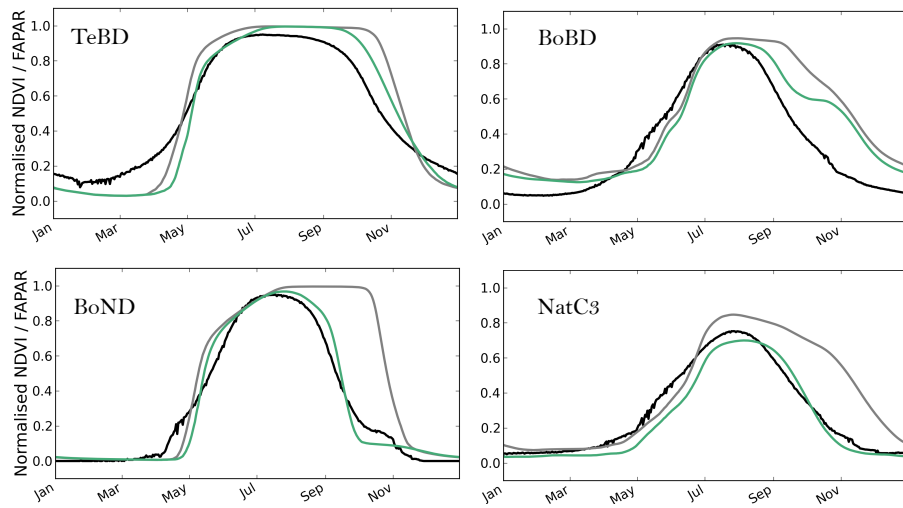
6

7



8

9 Figure 3: Location of the different observations used for each data stream assimilated in the
 10 system: MODIS-NDVI measurements, FLUXNET sites with NEE and LE measurements and
 11 atmospheric CO₂ stations (both the sites that aer assimilated and the sites used for the
 12 validation).

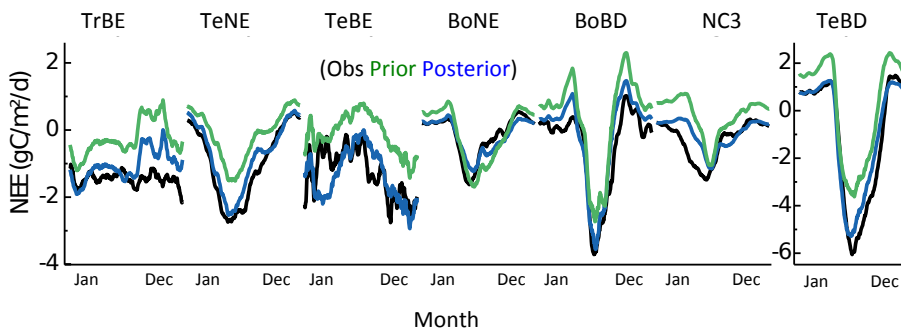


1

2 Figure 4. Mean seasonal cycle (2000-2008) of the normalised modelled FAPAR before and
 3 after optimisation, compared to that of the MODIS NDVI data, for the temperate and boreal
 4 deciduous PFTs (TeBD, BoBD, BoND and NatC3). Black = MODIS NDVI data; Grey =
 5 prior simulation (default ORCHIDEE parameters); Green = posterior multi-site optimisation.

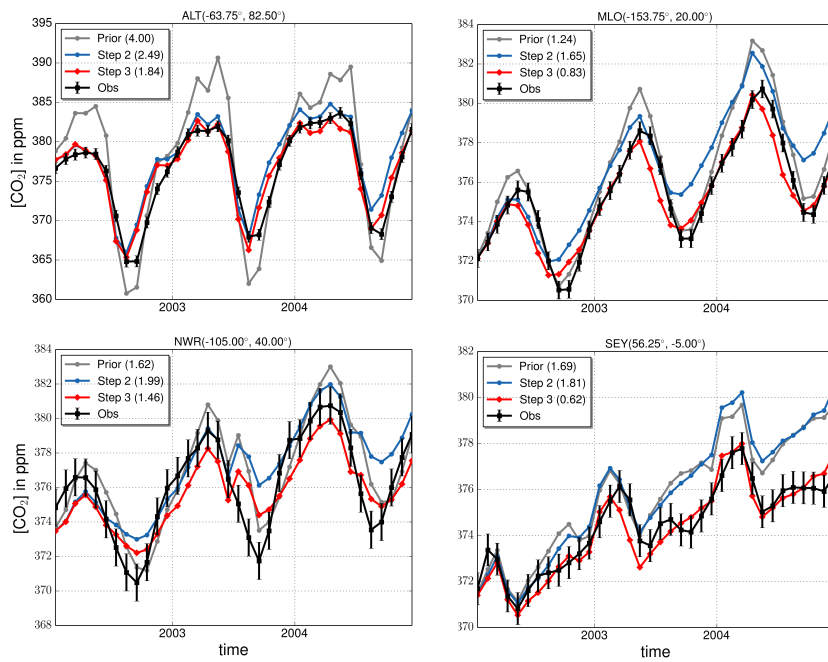
6

7



8

9 Figure 5: Mean seasonal cycle of the Net Carbon Ecosystem Exchange (NEE) for the
 10 different plant functional type optimized in Step 2 of the assimilation. The mean across all
 11 sites for a given PFT is provided for the observations (black), the posterior of step 1 (green)
 12 and the posterior of step 2 (blue).



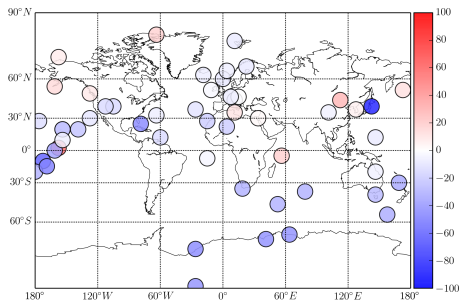
1

2 Figure 6: Monthly mean atmospheric CO₂ concentrations after step 3 of the optimization, for
 3 several stations over the period 2002-2004 of the optimization. The observations (black), the
 4 prior model (grey) and the posterior model after step 2 (blue) and step 3 (red) are displayed.
 5 Numbers in parenthesis correspond to RMSEs.

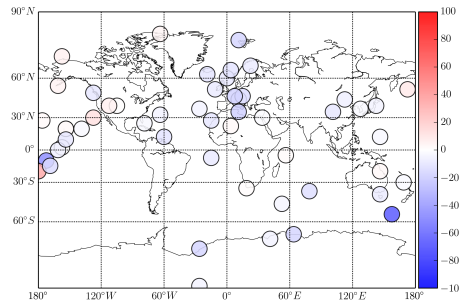
6

7

a) Seasonal amplitude: relative changes



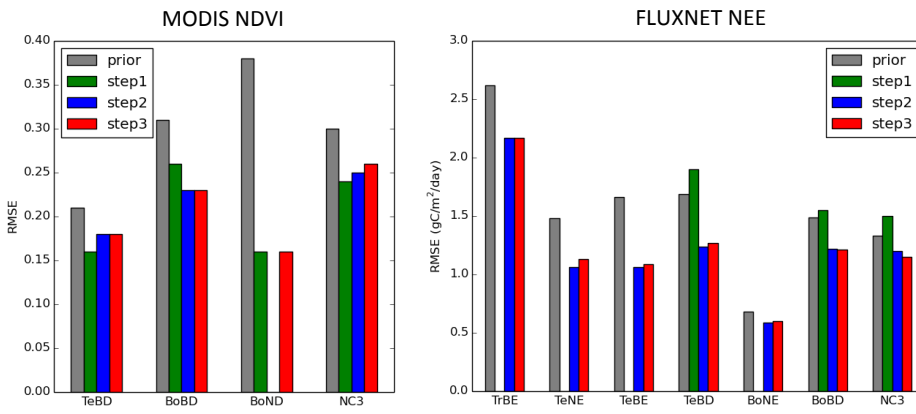
b) Length of CUP: relative changes



8

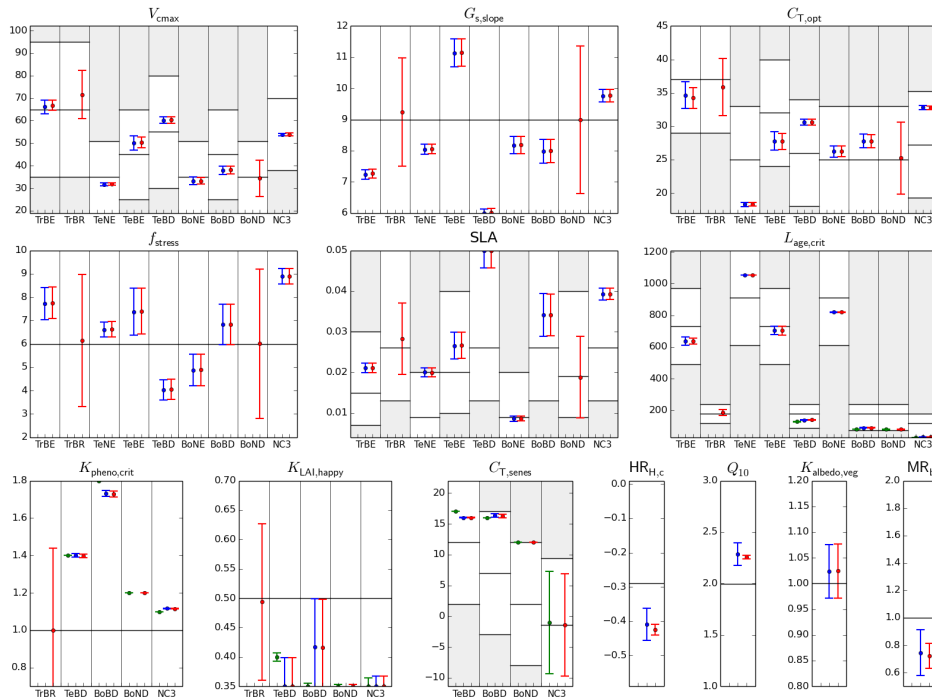
1 Figure 7: Changes in the mean seasonal cycle of the atmospheric CO₂ concentrations after
 2 step 3 of the optimization at all atmospheric stations. Left: Relative changes (in percentage)
 3 between the prior of step 3 and posterior absolute model-data differences for the amplitude of
 4 the seasonal cycle. Right: Same metric but for the length of the Carbon Uptake Period (CUP),
 5 measured as the sum of the days when the de-trended concentrations are negative (see text).

6
7
8



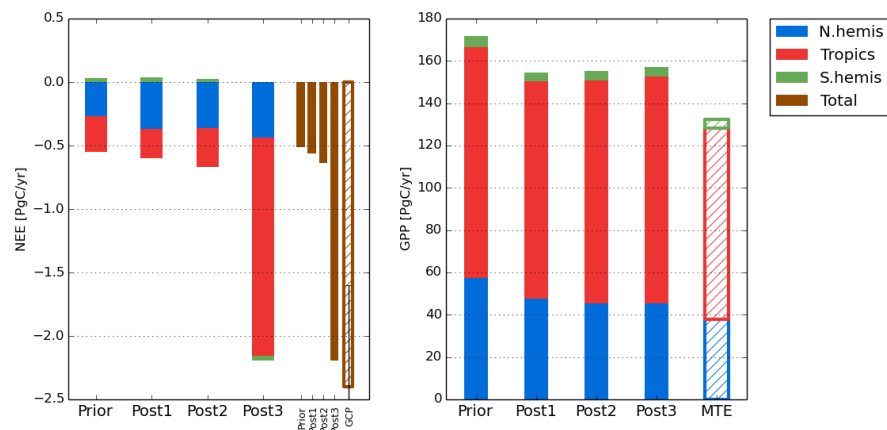
9
10 Figure 8: RMSE between model outputs and observations for two types of observations:
 11 MODIS-NDVI on the left and FluxNet-NEE on the right, for different Plant Functional
 12 Types (PFT: TrBE, TeNE, TeBE, TeBD, BoBD, BoND, NC3) and for the prior model simulation
 13 and the posterior of each step of the assimilation framework. Missing bars correspond to the
 14 fact that no data were available to constrain a given PFT.

15



1
2 **Figure 9:** Prior and posterior parameter values and uncertainties for a set of optimized
3 parameters (9 PFT dependent and 4 non-PFT dependent). The prior value corresponds to the
4 horizontal black line and the physical allowed range of variation to the “y” range (i.e. the
5 white zone). For PFT-dependent parameters, there are 9 sub-plots corresponding to PFTs that
6 were optimized (except for $K_{pheno,crit}$ with only 5 PFTs). For each parameter, there are 3
7 estimated values for the three successive steps: step1: assimilation of MODIS-NDVI data
8 (green symbol); step2: adding FLUXNET data (blue symbol); step3: adding atmospheric CO_2
9 data (red symbol). The parameter values are depicted with the symbols and the estimated
10 uncertainties with the vertical line (\pm sigma).

11
12
13
14
15
16
17
18



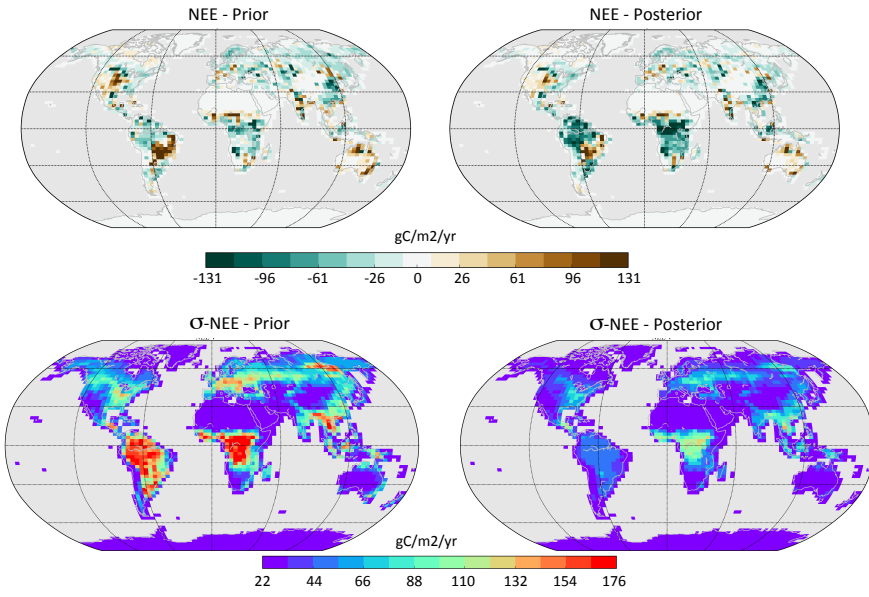
1

2 Figure 10: Left: Net Ecosystem Exchange (NEE) for three regions (North of 35°N, Tropics,
 3 South of 35°S) for the prior model, and after each step of the optimizations (mean over 2002-
 4 2004). The total NEE is indicated with the vertical brown bar and compared to the Global
 5 Carbon Project (GCP) estimate for the same period (Le Quéré et al. 2015). Right: same but
 6 for Gross Primary Production where the data driven estimate (MTE product using FluxNet
 7 data; Jung et al., 2009) is provided for comparison.

8

9

1



2

3 Figure 11: Simulated annual net carbon exchange (NEE) for the land ecosystems prior to any
4 optimization (left column) and after step 3 of the optimization process (right column). Upper
5 figures correspond to the mean NEE (in $\text{gC}\cdot\text{m}^{-2}\cdot\text{y}^{-1}$) over the assimilation period (2001-2003)
6 and lower figures to the associated monthly flux uncertainties (averaged over the whole
7 period and expressed in $\text{gC}\cdot\text{m}^{-2}\cdot\text{y}^{-1}$) due to the parameter uncertainties (see text).

8

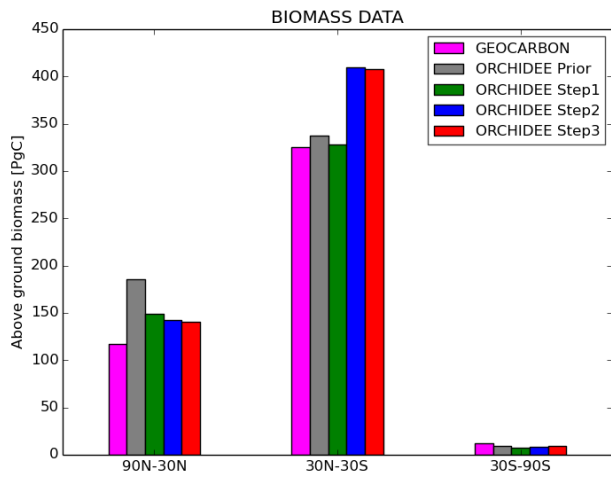


Figure 12: Above ground forest biomass data for the prior ORCHIDEE model and after step 1, step 2 and step 3 of the optimization process. Estimates from satellite observations (Santoro et al., 2015) and referred as “GEOCARBON” (following the EU-GEOCARBON project) are provided for comparison.

Appendix figures

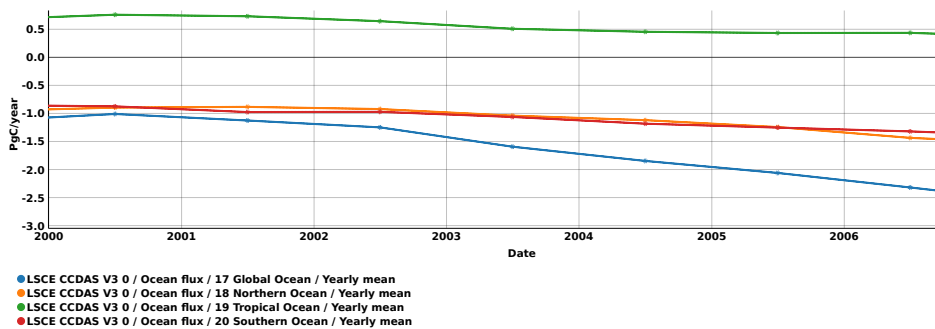
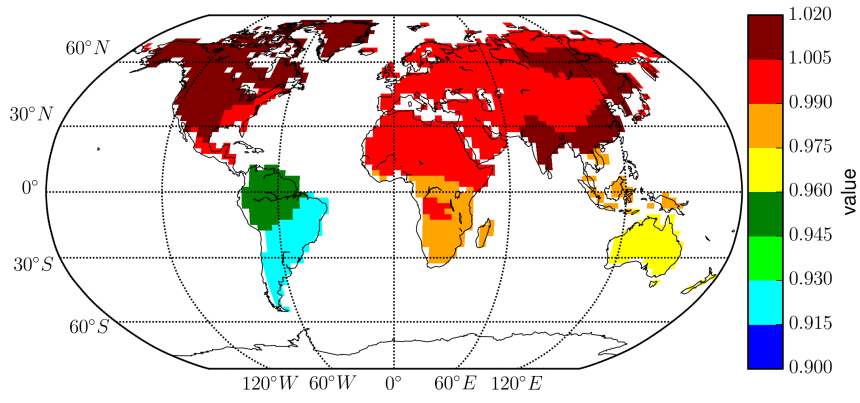


Figure A1: CO₂ air-sea fluxes including the natural ocean out-gazing, used as input to the ORCHIDEE-CCDAS and estimated from a neural network approach using observed pCO₂ data (see main text, section 2.5.1). The Northern, Tropical and Southern ocean contributions to the global ocean flux (blue curve) are also provided.

1



2

3 Figure A2: Map of the posterior values of the coefficient scaling the initial carbon pool sizes
4 per regions.

5

6